Analysis of 3 years of precipitation measurements from the Micro Rain Radar located at the Geophysical Institute

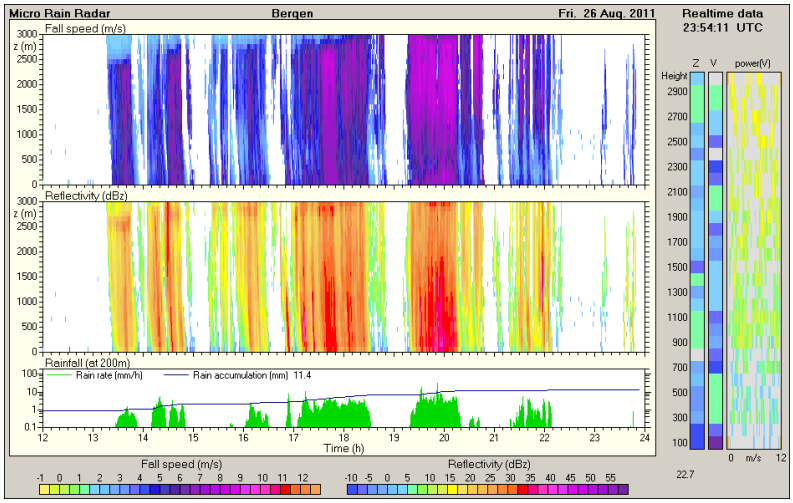

Master's thesis in meteorology

Lillian Bergheim

November 2013

University of Bergen
Geophysical Institute

Acknowledgements

This thesis has been an interesting and challenging experience for me and I have met lots of both motivational and computer challenges along the way.

First of all, I would like to express my gratitude to my supervisor Joachim Reuder for presenting this idea to me and for guiding me through this thesis. A big thanks for beeing able to squeeze me in, even just for 10 minutes in an otherwise full shedule.

I would also like to thank Tobias for helping me with a script for reading all the MRR data into Matlab. A big thanks to Torbjørn for helping me with all the computer challenges and thanks to Ragnhild and Smiti for proofreading and good ideas.

And last but not least thanks to all of you whom I have asked questions and received help from during these years as a student at the Geophysical Institute.

-Lillian

Contents

Abstract

An analysis of three years of vertically pointing Micro Rain Radar (MRR) data from the measurement platform at the Geophysical Institute has been performed. The measurement period started at 13.04.2010 and ended at 12.04.2013. The main motivation was to investigate the performance of the MRR in comparison to the rain gauge measurements by MET Norway and to investigate the validity of the Z-R relationships published in literature for the situation in Bergen. A comparison of the MRR and gauge raw data showed an annual overestimation by the MRR of 17 %, composed by a distinct overestimation of precipitation by the MRR in the cold season and an underestimation in the warm season. Based on 3 h precipitation amounts separated by the air temperature at Florida, the largest overestimation by a factor 2-2.5 was found for temperatures between 0 –3 °C. At this temperature interval the melting layer with its increased reflectivity is likely to be located in the range bin for rain rate determination. For temperatures above 6 °C an underestimation of 25 –30 % occurs more or less independently of temperature. The a-and b-values in the Z-R relationship showed a large variability, not only on a seasonal and synoptic scale, but also from hour to hour. For the overall three year period the a-values vary between 0 and 1000 and the b-values vary mainly between 0 and 2. The overall mean and median values of a and b can not fully confirm the reported values in the literature. The a-values are generally in the mid-range of the published ones, but the b-values are on average distinctly lower.

CHAPTER 1

Introduction

Precipitation is without doubt one of the key elements of the weather along the Norwegian west coast where moist Atlantic air masses are transported towards the mountains. The annual precipitation amounts can reach values up to 5000 mm, with an annual average of 2250 mm in Bergen (Geofysisk Institutt, n.d.), providing an economically important source of hydropower, but also causing frequent flooding and landslides in the area. Accurate forecasts and measurements of precipitation are therefore essential for this region.

However, precipitation is a parameter that is relatively hard to predict, particularly in areas with complex topography, as the Norwegian west coast (Young et al., 1999; Crochet et al., 2008). The improvement of numerical weather prediction models requires a better understanding of precipitation microphysics and good precipitation measurements for validation purposes. In general, precipitation measurements are subject to several problems. Rain is not evenly distributed over larger areas. It has a high spatial variability and point measurements does therefore not represent precipitation over large areas very accurately (Clark and Slater, 2006). The sampling efficiency of rain gauges decreases with increasing wind speed as rain droplets are transported around the measurement gauge instead of falling into it. Additional sources of error in light rain are evaporation from the gauge and wetting of the inner

walls (Nešpor and Sevruk, 1999). Some underestimation in heavy rain can occur because the rainfall is not measured during the time it takes for the tipping mechanism to empty and turn from one side to the other (Duchon and Essenberg, 2001).

Scanning radar systems can give a good picture of the horizontal variability of precipitation, but they only give a raw quantification of the precipitation amounts as weak, moderate or heavy. The reason for this is that they are dependent on empirically based assumptions on the droplet size distribution to convert the measured reflectivity into an accurate rain rate.

The relationship between radar reflectivity, Z, and rain rate, R, has been investigated several times before, among others by Marshall and Palmer (1948), Waldvogel (1974) and Stout and Mueller (1968). This so-called Z-R relationship is usually described by the coefficients a and b in an equation of the form $Z = aR^b$. The reported Z-R relationships vary with location, season and synoptic situation (Stout and Mueller, 1968). However those publications also suggest relatively constant conditions over several hours of a rainfall event.

Vertically looking radars, such as the Micro Rain Radar (MRR) used in this thesis, are able to provide this Z-R relationship instantaneously as they can derive droplet size information from measurements of fall velocity calculated from a Doppler shift of frequency.

In April 2010 one MRR system was installed on the observational platform of the Geophysical Institute (GFI) in Bergen. Since then it has produced a nearly continuous time series of precipitation data that is the basis for this work.

A main motivation for this thesis is to investigate the performance of the MRR in comparison with well established rain gauge measurements performed by MET Norway and to test how the Z-R relationships published in the literature correspond with those derived for Bergen. Overestimation of precipitation by radars during the cold season has been reported earlier, (Kneifel et al., 2011), another task will thus be to recognize situations when this happens and to quantify this effect.

A short introduction of general radar theory and the measuring principle of the MRR can be found in chapter 2. More information about the MRR, the rain gauge from MET Norway, datasets and methods can be found in chapter 3. Chapter 4 presents the results of the comparisons between rain

rates from the MRR and MET Norway. How different synoptic situations affect the relationships between a-and b-values and rain rates are investigated by three case studies in chapter 5. Finally, chapter 6 contains a summary and a short outlook.

CHAPTER 2

Theory and background

2.1 Basic Radar theory and history

RADAR, RAdio Detection And Ranging, is an active remote sensing method based on radio waves. It was first developed to discover and monitor approaching ships or airplanes, but a problem that occurred was precipitation blocking the view by attenuating the radar beam. As early as February 1941 the radar was first used to look at precipitation intentionally (McNoldy, 2003).

When radiation emitted by the radar (figure 2.1) hits a raindrop or some other form of precipitation some of the radiation is absorbed by the hydrometeor and the rest is scattered. A small part of this scattered radiation will return to the radar and carries information on size, velocity and phase (water or ice) of the hydrometeors.

A variety of frequencies are in use by meteorological radars and different frequencies are capable of detecting different sizes of objects, as aeroslos, raindrops, birds and airplanes. Short wavelengths are easier attenuated than longer wavelengths and are mostly used to detect clouds and aerosols. Longer wavelengths can not see the smallest targets (table 2.1).

A vertical pointing radar can, compared to a horizontal scanning radar, determine not only reflectivity but also fall velocities. This makes it possible

Band	f, [GHz]	λ, [cm]	Comments
W	90	0.1	W and K: High frequency, fast attenuation. Most usefull for detecting clouds and aerosols.
K	30	1.0	
X	10	3.0	Able to detect light rain and snow, often used for observations of cloud development.
C	5	6.0	Easily attenuated, mostly applicable for short range weather observations.
S	3	10.0	Used by the National Weather Service, high sensitivity and minimal attenuation. Can not see clouds.
L	1.5	20.0	Detection of rain, hail and larger targets as birds and planes. Can not see the smallest targets.

Table 2.1: Weather radar bands. f is the frequenzy and λ is the wavelength.

to determine rain rates more accurately. A horizontal scanning radar assumes a relationship between reflectivity and rain rate. This Z-R relationship, details in section 2.2.5, varies from situation to situation. This is the reason why the data from operational horizontal radar systems are usually not presented as accurate rain rates in $\mathrm{mm\,h^{-1}}$ but classified as weak, moderate or heavy. An example of a horizontal scanning radar image is given in figure 2.2.

2.1.1 The radar equation

The backscattered power the radar receives is given by the radar equation, 2.1.

$$P_e = \frac{P_s G^2 \lambda^2 \sigma}{(4\pi)^3 R^4} \tag{2.1}$$

Where P_s: transmitted power, G: antenna gain, σ: radar cross section, λ: transmitters wave length and R: range

For spherical droplets with a small diameter compared to the wavelength of the radar, $D < \lambda/16$, the area of backscatter by the droplets is given by the Rayleigh backscatter relationship:

$$\sigma_i = \frac{\pi^5}{\lambda^4}|K|^2 D_i^6$$
$$where |K|^2 = |\frac{\epsilon - 1}{\epsilon + 2}| \tag{2.2}$$

$|K|^2$ is the refractive index, water and ice has refractive indices of 0.92 and 0.18 respectively (METEK, 2004). ϵ is the dielectricity constant = 80.4 for water at 20 °C. D is the diameter of the droplet measured in mm.

In our case the wavelength of the Micro Rain Radar, MRR, is 12.5 mm, which means that $D < \lambda/16$ is not fulfilled for the whole range of rain drop sizes. Because of this and the fact that the larger droplets are not spherical due to deformation when they fall, Mie-scatter is required. Figure 2.3 shows the ratio between Mie and Rayleigh particle cross section scattering with respect to drop size, used by the MRR to retrieve drop sizes.

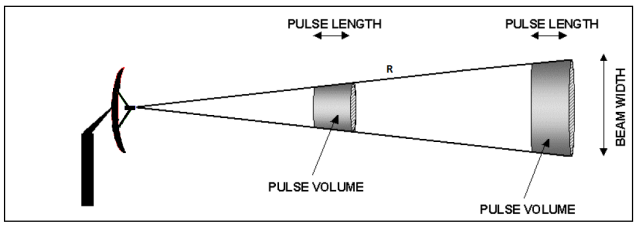

Figure 2.1: Principle of operation of a pulsed RADAR system. (McNoldy, 2003)

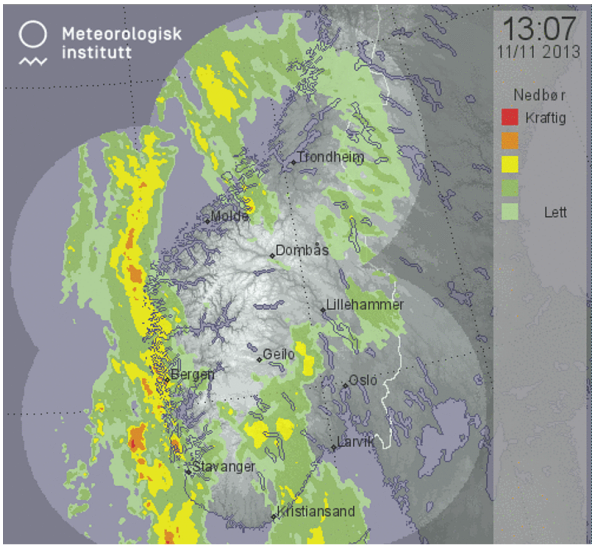

Figure 2.2: Example of a horizontal scanning radar image showing the location and intensity of the precipitation. (Source: http://www.yr.no/radar)

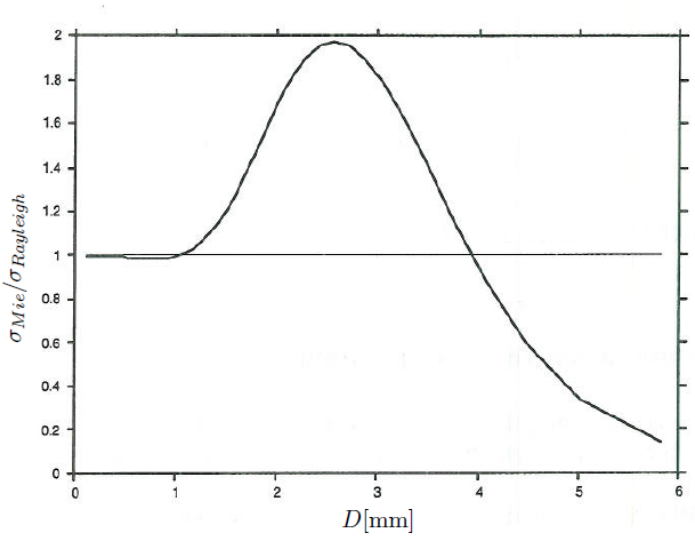

Figure 2.3: The single particle scattering cross section, relative to the Rayleigh approximation, as function of drop size used in the MRR retrieval algorithm (METEK, 2004).

2.2 Measurement principle of the MRR

2.2.1 Backscattered power

The raw spectral power received by MRR is given by the radar equation in the form:

$$p(f_D)\Delta f_D = C(r)\frac{1}{r^2}\frac{1}{\Delta h}\frac{\eta(f_D)}{\Delta f_D} \tag{2.3}$$

where Δh is the range resolution, r is the number of range gates, $C(r)$ is a calibration function, $\eta(f_D)$ is the spectral reflectivity and Δf_D is the frequency resolution of the 2^{nd} fourier transformation $= 30.52\,\text{Hz}$. The calibration function contains parameters specific to the radar, as transmitted power, antenna gain and the transfer function of the MRR radar receiver.

When radiation emitted from the MRR hits a raindrop, snowflake, hail or some other form of precipitation, radiation with a different frequency is reflected back to the MRR, $\eta(f_D)$. The backscattered frequency is different from the emitted signal due to vertical motion of the hydrometeors. This movement towards (or away from) the radar causes what is known as a doppler shift of frequency. This shift of frequency makes it possible for the MRR to calculate drop spectra, liquid water content, reflectivity and rain rates.

2.2.2 Drop Spectrum, N_D

The drop size distribution, i.e. the number of drops per volume and diameter, N_D, is given by equation 2.4 and is a function of spectral reflectivity, $\eta(D_{nn})$, and the backscattering cross section, $\sigma(D_{nn})$.

$$N(D_{nn}) = \frac{\eta(D_{nn})}{\sigma(D_{nn})} \tag{2.4}$$

(METEK, 2004). The subscript nn indicates the corresponding range bin.

$$\eta(D_{nn}) = \eta(f_{D,nn})\frac{\partial f_D}{\partial v}\frac{\partial v}{\partial D} \tag{2.5}$$

(METEK, 2004). $\eta(D_{nn})$ is, as can be seen in equation 2.5, dependent on the reflectivity measured by the MRR, how the doppler frequency changes with fall velocity and how the fall velocity changes with size of the droplet. Equation 2.6 shows the relation between fall velocity and size of the droplets, used by the MRR algorithm.

$$\begin{aligned} v(D) &= (9.65 - 10.3 \cdot exp(-0.6 \cdot D))\delta v(h) \\ \delta v(h) &= 1 + (3.68 \cdot 10^{-5}) + (1.71 \cdot 10^{-9} h^2) \end{aligned} \tag{2.6}$$

It is valid for $0.109\,\text{mm} < D < 6\,\text{mm}$.

As earlier mentioned, $D < \lambda/16$ is not fulfilled for the MRR and Mie theory is required for calculation of $\sigma(D)$ in equation 2.4.

Waldvogel (1974) found that "large-drop spectra are associated with widespread rain with a very pronounced bright band, whereas the small-drop spectra is associated with a cold front thunderstorm". More about the bright band and its features can be found in section 2.3

2.2.3 Characteristic fall velocity of droplets, W

The characteristic fall velocity of droplets is given as

$$W = \frac{\lambda}{2} \int_0^\infty \eta(f) f df \Big/ \int_0^\infty \eta(f) df \tag{2.7}$$

METEK (2004), where $\eta(f)$ describes the spectral reflectivity.

One characteristic fall velocity is given for each height interval of the MRR. Terminal velocity is the fall speed of a droplet when the gravitational force pulling the droplet downward equals the buoyancy force (Gunn and Kinzer, 1949), equation 2.6. The fall velocity varies with the size of the droplets and big droplets fall faster than small droplets. The terminal velocity of typical rain drops ranges between $9\,\text{m}\,\text{s}^{-1}$ and $13\,\text{m}\,\text{s}^{-1}$, (e.g. Beard (1976)).

2.2.4 Liquid Water Content

Liquid water content, LWC, is a measure of how much liquid water the air contains (Wallace et al., 2006). It is measured in grams per unit volume of air, $[\text{g}\,\text{m}^{-3}]$ and depends on the size of the droplets, D, and the number of drops in this volume of air, N(D), with diameter between D and $D + dD$.

$$LWC = \rho_w \frac{\pi}{6} \int_0^\infty \text{N(D)D}^3 \, dD \tag{2.8}$$

METEK (2004)

2.2.5 Reflectivity and rain rate

The relationships between radar reflectivity, Z, and rain rate, R, is a complex relationship that has been investigated multiple times in the years that have passed. Both Z and R depends on the drop size distribution (Huggel et al., 1996) and are given as equation 2.9 and equation 2.10 respectively. R is measured in $\mathrm{mm\,h^{-1}}$ and Z is measured in $\mathrm{mm^6\,m^{-3}}$.

Linear and exponential equations have been found and attempted to fit measurements of reflectivity and rain rate and some of this variation reported in the literature can be seen in table 2.2. By using the Marshall-Palmer exponential drop-size distribution (equation 2.11) (Marshall and Palmer, 1948), assuming $N_0 = 0.08cm^{-4}$ and $\Lambda = 41R^{-0.21}cm^{-1}$ and substituting this into equation 2.9 we end up with a relationship between Z and R, equation 2.12.

$$Z = \int_0^\infty \mathrm{N(D)D^6}\, dD \tag{2.9}$$

METEK (2004), .

$$R = \frac{\pi}{6} \int_0^\infty \mathrm{N(D)D^3v(D)\,dD} \tag{2.10}$$

METEK (2004), v(D) is the terminal velocity, measured in $\mathrm{cm\,s^{-1}}$ of a drop of diameter D.

$$N(D) = N_0 e^{-\Lambda D} \tag{2.11}$$

$$Z = N_0 \frac{6!}{\Lambda^7} = 296R^{1.47} \tag{2.12}$$

Written in a more general way as

$$Z = aR^b \tag{2.13}$$

Z given in equation 2.9 must not be confused with the z given in table 3.1. The z value given in the table is expressed in a logarithmic scale dBz, while Z in 2.12 is not. Converting from logarithmic scale to "normal" scale (Huggel et al., 1996):

$$\begin{aligned} z &= 10log(Z) \\ Z &= 10^{\frac{z}{10}} \end{aligned} \tag{2.14}$$

The coefficients a and b in the Z-R relationship vary from one situation to another. Their values "depend on the type of precipitation, the geographic location, season, the resolution in time of the data, and last but not least on the preferences of the scientist who introduces them" (Huggel et al., 1996). In Fujiwara (1967) it is mentioned that Louis J. Battan in 1965 found values of variable a varying from 17 to 600, and b-values varying from 1.24 to 2.87. During an experiment in Alaska in the 1950's it was concluded that radar-rainfall relationships changed from season to season and from day to day. It was also found that in hurricanes when the rain rate is high the reflectivity is low. The opposite seems to be the case in light to moderate rain situations (Stout and Mueller, 1968).

There are two different ways to determine the relation between Z and R, a direct approach and an indirect approach (Stout and Mueller, 1968). When using the direct approach the amount of rainfall is measured by a gauge at the ground and the reflectivity is measured by a radar. If both reflectivity and rain rate measurements are taken from the radar the method is said to be indirect. Both methods have advantages and disadvantages. One disadvantage of the direct approach is that the reflectivity is measured above the ground while the amount of rain is measured at the ground. The precipitation measured by the radar will often be larger than what is measured by the gauge in windy conditions. Reasons being that raindrops commonly follow wind trajectories around the gauge instead of falling into it. Another source of error is evaporation from the gauge. Some precipitation may stick to the walls of the gauge, and will thus not be counted (Nešpor and Sevruk, 1999). When measuring precipitation with a tipping bucket gauge, some underestimation occur in heavy rain because the rainfall is not being measured during the time it takes for the tipping mechanism to empty and turn from one side to another (Duchon and Essenberg, 2001).

One disadvantage of the indirect method is that the vertical velocity of the individual drops is needed to be able to calculate the rain rate (Stout and Mueller, 1968), equation 2.10. Strong updraft in the region around the radar will cause the droplets to fall slower than in stagnant air. This will affect

the backscattered signal and the radar will not be able to do a correct rain estimation.

Stout and Mueller (1968) carried out raindrop spectra measurements for a low pressure system in Florida, USA, but instead of making one Z-R relation for a whole synoptic system, or precipitation period, the system was divided into different parts and different relationships were derived for the various parts of the synoptic situation. The coefficient and exponent in the Z-R relation turned out different in a cold front than in a warm front, see table 2.2.

In table 2.2 some of the variation between $a-$ and b-values are shown. The equation found by Atlas (1957) contains both the highest $a-$ and b-value. Excluding this equation, the greatest value of a does not necessarily give the biggest b-value. The thunderstorm measurements reported by Waldvogel (1974) and Stout and Mueller (1968), are in the lower part of the range looking at a-values but close to or at the median looking at the b-values. Median a- and b-values in this table are 220 and 1.5 respectively. How these values change with precipitation rates are not mentioned in earlier studies, but will be looked into for three different precipitation events in chapter 5.

2.3 Bright band

Looking at the panel in the middle of figure 3.2 a bright red line can be seen at an altitude of 2300 –2500 m. This is known as the bright band where frozen particles melt, thus also known as the melting layer. Depending on the temperature of the air this bright band is closer to or further away from the ground and a good indication for the 0 °C - level in the atmosphere. The higher reflectivity in the bright band can be explained by a film of water forming on the frozen particles when they melt (Haby, n.d.). Snow is a better absorber of radiation than liquid water and more radiation will thus be reflected from the water covered snowflake than from a drier snowflake, located above the melting layer, or from a smaller melted droplet below the bright band. The radar interpret snowflakes, or other frozen hydrometeors, covered with liquid water as large raindrops and the amount of precipitation will therefore be overestimated (Klaassen, 1988).

Figure 2.4 presents a winter situation where the bright band stretches from the ground to a heigth of 400 m. This means that the bright band

Reference	Z = ($[mm^6m^{-3}]$)	Comments
Uijlenhoet and Pomeroy (2001)	$238R^{1.5}$	The mean of Battan (1973) relationship.
Marshall and Palmer (1948)	$296R^{1.47}$	Equation 2.12
Wilson and Brandes (1979)	$200R^{1.6}$	The most widely used Z-R relationship. Found by Marshall and Palmer.
Austin (1987)	$230R^{1.4}$ $400R^{1.3}$ $100R^{1.4}$	Mixture of rain, more or less average/ordinary rain. Intense convective cells Noncellular rain
List (1988)	$200R^{1.6}$ $742R$	Standard Marshall-Palmer Z-R relation. Linear relationship, steady tropical rain situations.
Waldvogel (1974)	$300R^{1.5}$ $85R^{1.5}$ $350R^{1.5}$ $150R^{1.5}$ $220R^{1.5}$ $170R^{1.5}$ $310R^{1.5}$	Used commonly in Switzerland. A fairly good approximation when the bright band is well defined and when the precipitation is uniform, (Huggel et al., 1996). Thunderstorm, Switzerland, 06.06.68. Widespread rain after the previous mentioned thunderstorm, Switzerland, 06.06.68. Shower, Switzerland, 19.06.69. Widespread rain following the shower on 19.06.69, Switzerland. Widespread rain, Switzerland, 26.05.69. Widespread rain, Switzerland, 26.05.69.
Stout and Mueller (1968)	$403R^{1.24}$ $198R^{1.24}$ $70R^{1.42}$	Warm front, Florida, USA. Cold front, Florida, USA. Thunderstorm in Ottawa, Canada.
Atlas (1957)	$1680R^{1.8}$	Curve fitted to six samples made in Lexington, Massachusetts 21.01.54.

Table 2.2: Continues

Reference	Z = ($[mm^6m^{-3}]$)	Comments
Kumar et al. (2011)	$330.74R^{1.25}$	Convective rain, Singapore, 09.01.98.
	$149.44R^{1.55}$	Transition stage between convective and stratiform rain, Singapore, 09.01.98.
	$182.61R^{1.43}$	Stratiform rain, Singapore, 09.01.98.
Fujiwara (1967)	$39R^{1.10}$	Hawaii, 23.08.65, 651 meters above sea.
	$45R^{1.07}$	Hawaii, 28.07.65, 1030 meters above sea.
	$230R^{1.68}$	Hawaii, 16.08.65, 715 meters above sea.
Fournier (1999)	$300R^{1.4}$	The primary default Z-R relationship used by the National Weather Service, USA, for the WSR-88D radar network

Table 2.2: Overview of previously found Z-R relations from the literature.

is located within the region where the radar estimates the rain rate at the ground. Consequently the MRR will heavily overestimate precipitation in this case. The bottom panel shows a rainfall of 64.4 mm registrated by the MRR between 0730 UTC and noon. For comparison, the Meteorological Institute measured 11.8 mm over the same 4.5 h period.

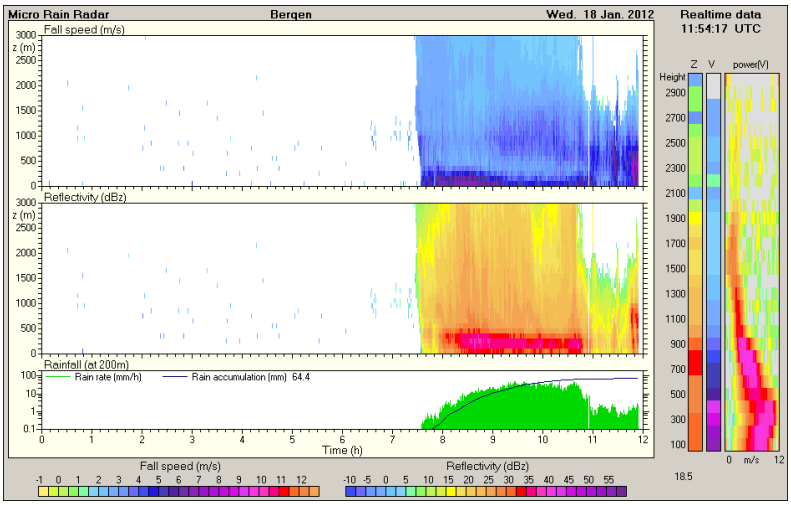

Figure 2.4: An example of precipitation overestimation by the MRR when the bright band is located in the range bin used for ground precipitation estimation.

In a stationary situation the same amount of water (frozen or not) that goes into the melting layer needs to come out from this volume of air. This conservation of mass gives us a fall velocity that is inversly proportional to the droplet number density, (Klaassen, 1988):

$$N(d)V(d) = const \tag{2.15}$$

N(d) is the number density, and V(d) is the fall velocity of hydrometeors. For equation 2.15 to be true, keeping the reflectivity constant, faster falling droplets needs to have smaller particle density than slower falling hydrometeors. This again means that because melting changes the fall velocity, drop size distributions below the melting layer will be different from the distribution above.

CHAPTER 3

Instrumentation, data and methods

3.1 Instruments

3.1.1 The Micro Rain Radar, MRR

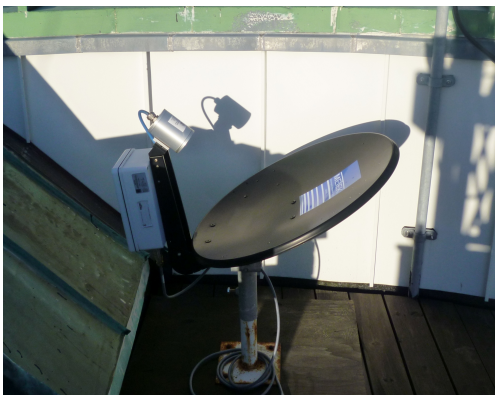

Figure 3.1: The MRR

The Micro Rain Radar, MRR, produced by METEK, is a vertically pointing remote sensing instrument which sends out electromagnetic radiation at a frequency of 24 GHz with a modulation that vary between 1.5 MHz and 15 MHz. A frequency of 24 GHz corresponds to a wavelength of $\lambda = 12.5$ mm. ($c = f \cdot \lambda$, where $c = 2.99 \cdot 10^8$ is the speed of light.)

The vertical resolution and number of range gates can be changed. However the maximum number is limited to 30 and height ranges greater than 200 m are not recommended for operational use (METEK, 2004). For the deployment at the Geophysical Institute (GFI), the vertical resolution of the MRR is set to 100 m and with 30 range gates the total measurable range extends to 3000 m above ground. The instrument is located on the measurement platform of the top of the GFI building at an altitude of 40 m above sea level.

When radiaton emitted from the MRR hits a raindrop, snowflake, hail or some other form of precipitation, radiation with a different frequency is reflected back to the MRR. It is this doppler shift of frequency that makes it possible for the MRR to determine the fall velocities of droplets and to calculate drop spectra and rain rates. See chapter 2.2.1.

Table 3.1 shows an example of the MRR data structure. The data are available at 1 minute intervals and stored in daily files consisting of 1440 $(24 * 60)$ similiar sections.

Every one minute data set begins with a header line. It contains date and time information followed by instrument and localization parameters, averaging time, vertical resolution, location above sea level, sampling rate, software version, serial number of the MRR and a calibration constant. The header line is followed by H, giving range heights, and a corresponding transfer function for each range bin, TF. Next comes 64 lines with information about the backscattered power, in dB, and 46 lines containing information about the drop spectra/drop size distribution. Based on this information the MRR calculates, for each height interval, the reflectivity, z, the rain rate, R, the liquid water content, LWC and the characteristic fall velocity of droplets, W. This information is then graphically displayed in form of 12 h plots, figure 3.2.

The top panel of figure 3.2 shows the vertical velocity of the hydrometeors. In this example an abrupt change of velocity takes place at an altitude varying between 2500 m and 2000 m. This is where the frozen particles melts and become faster falling rain droplets. The middle panel presents the radar reflectivity. A sharp red line can be seen at the level of velocity change. This visualizes the bright band, section 2.3, an area of enhanced reflectivity caused by the phase change of melting particles. The bottom panel shows the intensity of precipitation taken from the second range bin of the MRR, i.e.

MRR 130103065000 UTC AVE 60 STP 100 ASL 40 SMP 125e3 NF0 1.000 NF1 0.000 SVS 4.10 DVS 3.11 DSN 060702 CC 2430000													
H	100	200	300	400	500	600	700	800	900	1000	...	2900	3000
TF	0.0187	0.0530	0.1164	0.1965	0.2963	0.3950	0.4834	0.5748	0.6580	0.7443	...	0.7370	0.6435
F00	-73.08			-89.38				-88.99	-78.07	-70.15	...	-70.26	-67.86
F01	-75.40							-80.32	-73.79	-67.41	...	-72.90	-69.82
F02	-83.09						-87.43	-76.91	-71.39	-65.40	...	-78.58	-75.66
											...		
...											...		
											...		
F61			-82.66	-74.73	-80.27					-72.01	...	-79.37	-81.01
F62	-84.22		-86.24	-76.74	-84.93			-90.03	-83.68	-71.45	...	-76.36	-75.94
F63	-75.72		-98.05	-80.46				-91.42	-81.53	-71.38	...	-71.77	-70.16
N04	-9.5e3	-1.7e4	-1.8e4	-1.5e4	-4.3e4	-7.4e4	3.2e5	8.8e5	3.6e6	1.2e7	...		
N05	-7.3e2	0.000	-4.5e2	1.2e3	-1.8e3	0.000	1.8e5	4.9e5	2.0e6	6.2e6	...		
N06	1.3e3	3.8e3	5.3e3	4.0e3	2.7e3	9.0e3	1.0e5	2.9e5	1.2e6	3.3e6	...		
											...		
...											...		
											...		
N47	0.028	0.067	0.073	0.066	0.054	0.023	0.004	0.004	0.001	0.001	...		
N48	0.011	0.033	0.041	0.037	0.030	0.012	0.002	0.001	-0.000	0.000	...		
N49	0.004	0.016	0.023	0.021	0.018	0.007	0.001	0.000	-0.000	0.000	...		
z	33.5	34.6	33.9	33.2	32.6	31.9	31.6	32.5	34.8	33.4	...	10.2	14.6
RR	3.10	4.03	3.43	3.28	3.73	5.61	9.40	15.69	41.20	65.00	...	0.00	0.00
LWC	0.16	0.23	0.20	0.20	0.23	0.41	0.98	1.89	6.02	13.04	...	0.00	0.00
W	6.93	6.91	6.99	6.87	6.44	5.54	4.90	4.52	3.45	2.44	...	1.21	2.04

Table 3.1: MRR Data File. The following are removed for simplicity : line F03 to F60 (FFT spectra), line N07 to N46 (drop spectra), and columns with height steps from 1100 m to 2800 m.

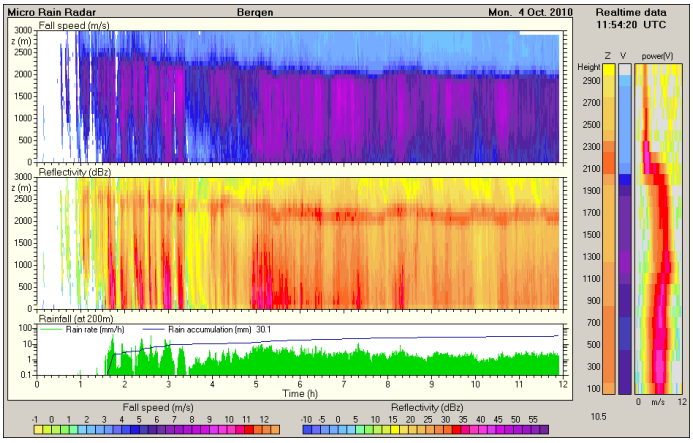

Figure 3.2: Hydrometeor fall velocity (upper panel), radar reflectivity (middle panel) and rain rate (lower panel) from the MRR measurements.

the height interval from 100 –200 m above the instrument.

3.1.2 Rain gauge used by the Meteorological Institute

Figure 3.3: The rain gauge from Geonor

The rain gauge used in the study is owned and operated by the Meteorological Institute and was deployed on the lawn in front of "Værvarslinga på Vestlandet" in February 2007. It is produced by Geonor and operates on a vibrating wire principle (Geonor, n.d.). The wire is vibrating at a given frequency. The frequency changes with the weight of the bucket. The instument has a collecting area of 200 cm^3, sensitivity of 0.05 mm and a repeatability of 0.1 mm.

3.2 Data

All data used are for the three-year period from 13.04.2010 until 12.04.2013.

3.2.1 MRR data

The MRR was set into operation 12.04.2010 at 1455 UTC. In this thesis three years of one minute values of reflectivity and rain rate are used, starting on 13.04.2010. There were some start-up problems with the MRR the first year related to data transfer and storage. This resulted in three periods of missing data: 19 - 28.05.10, 24 - 31.08.10 and 15 - 16.12.10. Even though the precipitation gauge from met.no is placed at the ground the lowest range gate from the MRR is not used due to greater risks of backscattering from trees and buildings (METEK, 2004).

3.2.2 Rain gauge data from MET Norway

From April 2010 to and including April 2011 the hourly precipitation data from MET Norway are not given directly as rain rates for every hour, but as hourly time series of accumulated precipitation. Hourly precipitation has been calculated by substracting subsequent values. Precipitation from the gauge is drained at irregular intervals. For those events zero precipitation over the last hour is assumed. All hours where the amount in the subsequent hour is less than the previous hour, subtraction gives negative rainfall, potentially due to evaporation from the gauge. These negative values are replaced with zero in the data sets. From May 2011 the precipitation is given as hourly values, but it still contains some negative values and some hours without measurements. Negative values are, as in the previous months, replaced by zero rainfall.

3.2.3 Florida and Ulriken data from GFI

In this project 10-minute values of wind speed, wind direction and temperature at Ulriken and Florida are used, in addition to 10-minute pressure information from the station at Florida. The wind sensor at Ulriken had some problems during autumn 2010 and some unphysical spikes in the wind speed measurements are substituted with NaN values in the datasets. This

will keep the dataset complete, but erroneous values will not be plotted and they will not impact means and sums incorrectly.

3.3 Data processing

3.3.1 MRR data files

The MRR stores, as previously mentioned, the one minute measurements in one large file for every day. The one minute values of reflectivity and rain rate for all height levels were read into Matlab and integrated over 10 min, 1 h and 3 h values for further evaluation.

3.3.2 Measurements of temperature, wind speed and direction

Three hour average values of temperature were made by summing hourly values and divide by the number of measurements, $\bar{x} = \frac{\sum x_i}{n}$. The 10 minute values of wind were decomposed into u- and v direction, u and v were averaged separately and afterwards recombined to the averaged wind vector $\overrightarrow{u}$.

$$\begin{aligned} u &= -windspeed * cos(\alpha) \\ v &= -windspeed * sin(\alpha) \\ \overrightarrow{u} &= \sqrt{u^2 + v^2} \end{aligned} \tag{3.1}$$

Where u is wind in x-direction, v is wind in y-direction, and α is the angle between north and the direction where the wind is comming from.

3.3.3 Z-R relationships

The raw data on reflectivity and rain rate measured by the MRR can be used to calculate the coefficients a and b in the Z - R relationship, $Z = aR^b$. Minute values of rain and reflectivity were used to determine a- and b-values for 1 h and 3 h intervals.

3.4 Statistics

3.4.1 Correlation coefficient, r

The correlation coefficient describes the strength of the linear relationship between two variables, here precipitation from MET Norway and from the MRR, and is defined as $r = \frac{S_{xy}}{S_x S_y}$. S_x and S_y are the standard deviations of variable x and y respectively, and S_{xy} is the covariance between the variables. The value of r is always between 1 and -1. A positive correlation coefficient means that if variable x increases so does the variable y, or x and y both decreases. If x increases and y decreases, or vice versa, the correlation is negative. The stronger the linear relationship is between the two variables the closer the correlation coefficient is to 1 or -1. If the correlation coefficient is exactly one or minus one, all points will lie on a stright line in a scatter plot (Mendenhall III et al., 2006).

3.4.2 Coefficient of determination, R^2

The coefficient of determination is defined as the square of the correlation coefficient and is a number between 0 and 1. It indicates how much of the observed variability in the data set is explained by the linear relationship $y = ax + b$ (Mendenhall III et al., 2006).

CHAPTER 4

Results and analysis

In this chapter precipitatation measurements from the MRR will be compared to the measurements of the rain gauge operated by MET Norway. The relationship between reflectivity, Z, and rain rate, R, will be investigated through the equation $Z = aR^b$.

4.1 Annual accumulated precipitation

Figure 4.1 presents the precipitation measured by the MRR and the gauge operated by MET Norway. The different years are defined as: year 1: 13.04.2010 - 12.04.2011, year 2: 13.04.2011 - 12.04.2012 and year 3: 13.04.2012 - 12.04.2013. The precipitation measurements from the MRR is from the second range bin, i.e. 100 - 200 meter above the instrument. No adjustments for the precipitation overestimation by the MRR due to the location of the bright band in the lowest range bins have been applied on the MRR raw data. From this figure it is clear that the MRR measures more precipitation than the rain gauge on annual basis. A year to year variability is evident and the measurements from the MRR ranges from 2342 mm to 3777 mm, third and second year respectively. The first year lies in between with an annual precipitation rate of 2715 mm. The measurements from MET Norway ranges from 1991 mm the third year to 2862 mm the second year. The first year has a total of 2415 mm.

This means that for the first year the gauge measured 89 % of the total amount measured by the MRR . The second and the third year difference is bigger and the gauge measures 76 % and 85 % of the total amount measured by the MRR.

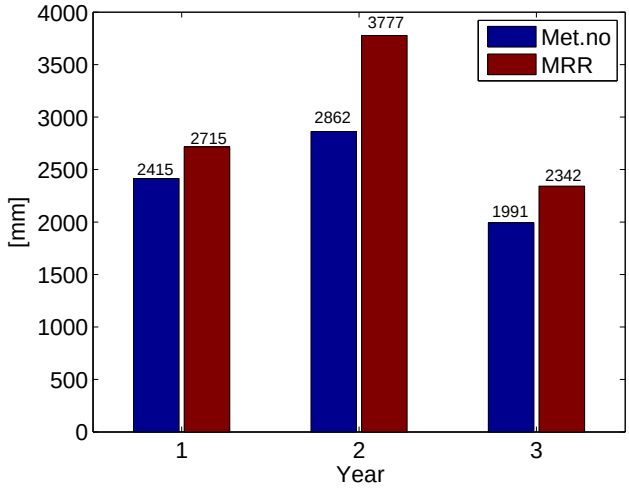

Figure 4.1: Annual amount of precipitation from MRR raw data and the MET Norway rain gauge. Years are defined from 13.04 to 12.04 the next year, starting on 13.04.2010.

Figure 4.2 shows the accumulated precipitation for each year. The result is the same as in the previous figure, i.e. that the MRR measures more precipitation annualy than the gauge from MET Norway. It is worth noting that in this figure the shape of the red and the blue lines are almost identical. When one of them increases the other one does the same, but not always by the same amount. During summer and autumn the MRR measures less precipitation than the gauge. This is mostly pronounced during year 1 and year 2 where the red line has a significantly smaller slope than the gauge measurements from the start, but increases rapidly during the winter and passes the measurements from MET Norway on February 2^{nd}, 2011 and Desember 16^{th}, 2012. The smaller slope of the red line is also evident in year 3, but here seen as a decreasing gap between the red and the blue line until the end of October. After this the gap between the lines increases again, meaning the MRR measures more than the gauge from MET Norway. This is a clear expression of the overestimation of precipitation by the MRR as a

result of the frequent location of the melting layer close to the surface during the cold season, see section 2.3.

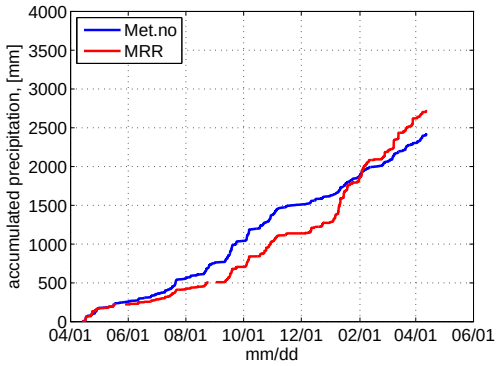

(a)

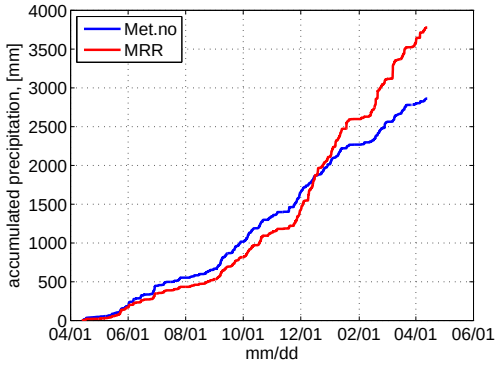

(b)

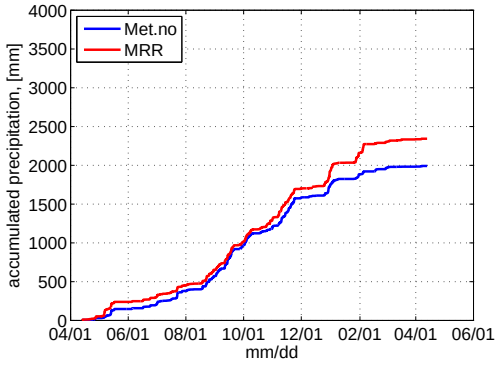

(c)

Figure 4.2: Accumulation of rain, (a) first year: 13.04.2010 - 12.04.2011, (b) second year: 13.04.2011 - 12.04.2012, (c): third year: 13.04.2012 - 12.04.2013.

4.2 3 h rain rates

3 h rain rates measured by the Meteorological Institute plotted against the precipitation measured by the MRR give an indicator of how well the different measurements correspond on a shorter time scale. Measurements that are exactly the same should be located at the line $y = x$. Figure 4.3 shows 3 h precipitation amounts from MET Norway and the MRR plotted against each others. In (a) for the overall 3 year period, in (b), (c) and (d) for the individual years. In all four figures the best fit line between the points are quite close to $y = x$, with slopes varying between 0.94 and 0.99. Even though the slope of the regression is fairly good, there are still many points that are located far away from the 1:1 line, especially at the left side, close to the y-axis. The coefficients of determination are found to vary between 0.25 and 0.57, see also table 4.2. This means that only between 25 % and 57 % of the variability can be explaned by the linear relationship $y = ax + b$.

To get a better understanding of why the best fit equations shows a good relationship between the measurements from the MRR and from MET Norway but low coefficients of determination, the data sets were separated in temperature intervals according to ground temperature at Florida. This was done under the assumption that the largest deviations are caused by the occurence of the melting layer in the lowest range bins. For that the air temperature at Florida provides the best available source of information. The result can be seen in figure 4.4, in (a) for the overall 3 year period, in (b), (c) and (d) for the individual years. In these figures the regression lines for all temperature intervals below 6 °C are located towards the y-axis. The steeper slope is an expression of the on average overestimation of precipitation in this temperature inverval by a factor of around 2. The regression line for all temperatures above 6 °C are located to the right of the 1:1 line. In general this underestimation has a value of around 25 % and is independent of temperature. Some year to year variability can be seen, but in general all years behave in a similar way.

For the overall 3 year period the temperature interval of 0-3 °C has the biggest overestimation with a factor of 2.17. This is the temperature interval where it is most likely to have the bright band in the range bin where the MRR estimates the rain rate. This overestimation decreases for the temperature intervals above and below, with factors of 1.43 and 1.91 respectively.

The coefficient of determination for the three year period has a minimum value of 0.27 for the temperature interval of 0 –3 °C. This minimum value indicates a high variability among the MRR and MET Norway precipitation measurements and it is in this region the highest probability of wet, water covered snowflakes occur. The coefficient of determination increases with increasing temperatures and reaches a maximum of 0.83 for temperatures above 9 °C. It also increases when the temperature drops below 0 °C and has a value of 0.59. For temperatures below freezing the precipitation comes mostly as pure snow, indicating a decrease in uncertainty due to the melting layer. Some year to year variability is evident, but in general the same behavior can be seen. For example for year 3 the coefficient of determination states that as much as 90 % of the variability above 9 °C is explained by the linear relationship $y = 0.83x + 0.10$.

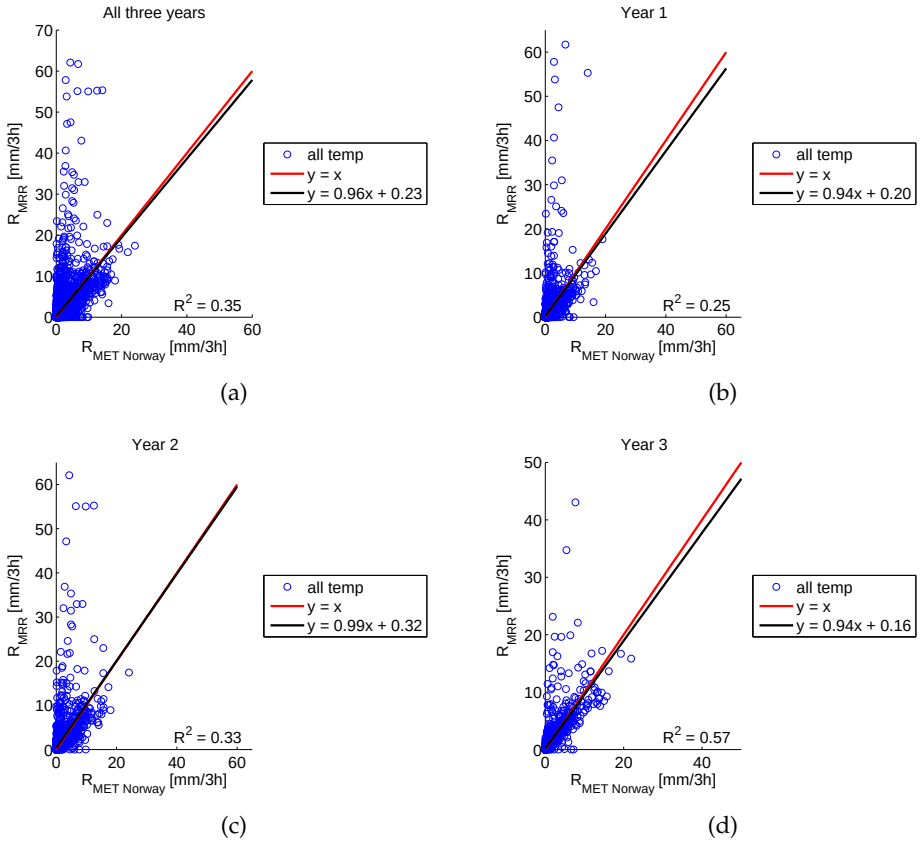

Figure 4.3: 3 h precipitation measured by MET Norway vs. precipitation measured by the MRR. R^2 is the coefficient of determination.

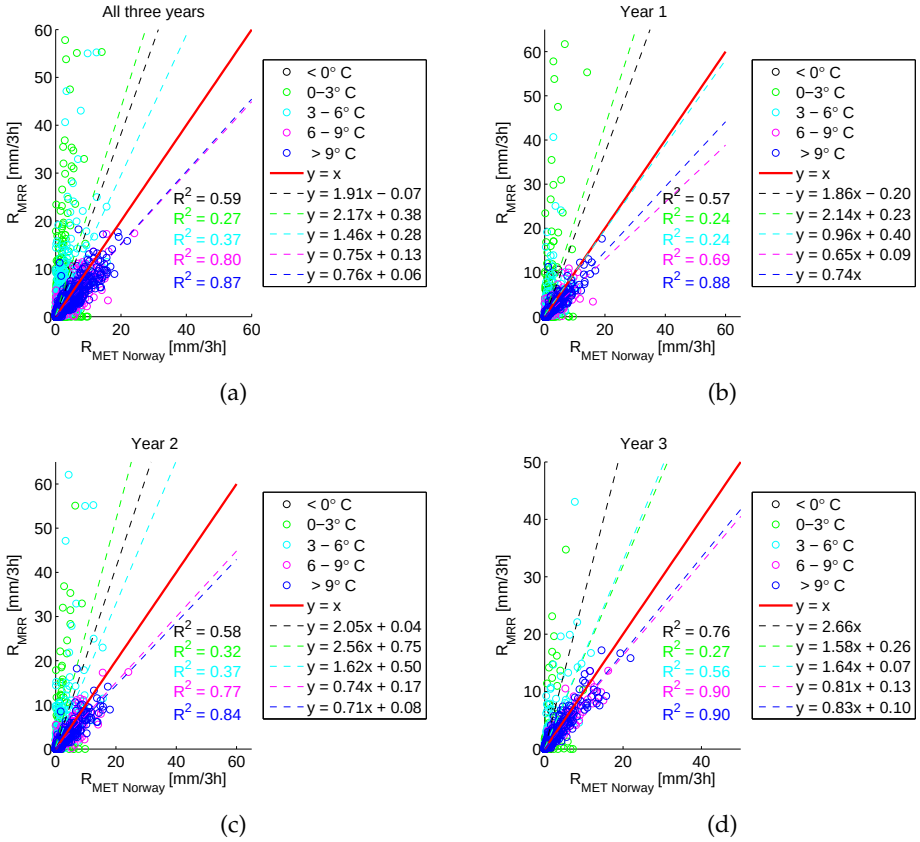

Figure 4.4: 3h precipitation measured by MET Norway vs. precipitation measured by the MRR. Rain rates are separated by the air temperature at Florida. R^2 is the coefficient of determination.

4.3 Filtering the MRR data

Until now all data points have been included in the figures, also the periods with no or almost no precipitation. This large number of data points have most likely affected the statistics of figure 4.3 and 4.4. The coefficients of determination are expected to show a relationship that is better than they would have been if the periods without precipitation were not included. These data points will most likely also force the intersection point with the y-axes downwards towards the origin, compared to if they would have been removed. In this chapter an objective method for removing the times with no precipitation from the data set is investigated. This is done by looking at the probability density distribution of the parameters a and b in the Z-R relationship.

Figure 4.5 and 4.6 shows the distribution among a- and b-values in the Z-R relationship, $Z = a R^b$, based on intervals of 3 h. The histograms are divided into the same temperature intervals as figure 4.4.

In 4.5 (a) where no separation due to temperature is done, a singular peak at $a = 1$ can be seen. A second peak is evident at an a-value of 20-30, a steep decrease is evident between 30 and 50. From here a more or less continuous decrease towards 600 can be seen, except some local maxima between 200-300. In (b) - (f) where separations are done due to ground temperature at Florida, one can see that the peak of a-values below 50 is clearly associated to the lower temperatures. For temperatures less than 3 °C, nearly no a-values above 200 are evident. As the temperature increases so does the range of a-values. In general the probability of occurrence decreases with increasing values of a.

Figure 4.6 shows a clear bimodal distribution with a distinct separation between the minor and major modes at b-values of 0.2. The distribution for the major mode of b-values looks nearly symmetric for all cases, except in (b). In (b) - (f) it looks as if the peak of the major mode moves towards higher b-values for increasing temperatures.

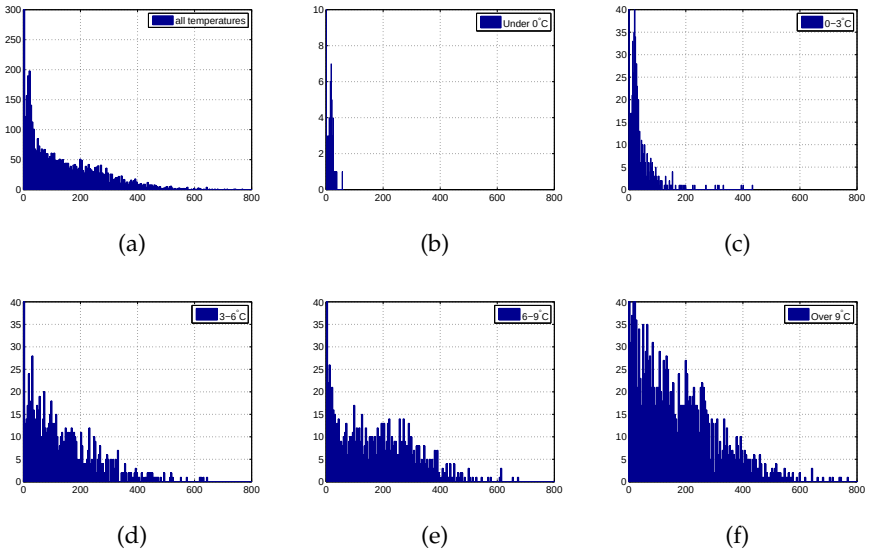

(a) (b) (c)

(d) (e) (f)

Figure 4.5: $Z = aR^b$. a-values separated by the temperature at Florida. Note the different ranges of the y-axes.

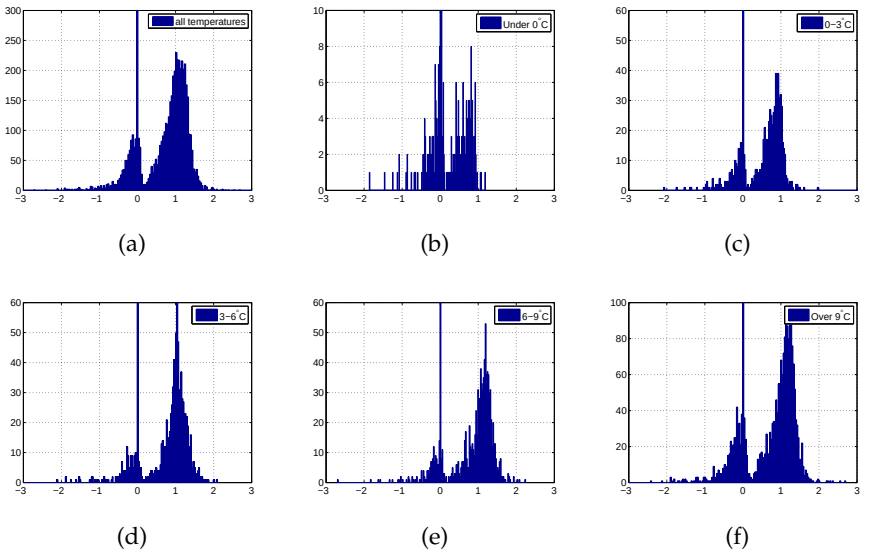

(a) (b) (c)

(d) (e) (f)

Figure 4.6: $Z = aR^b$. b-values separated by the temperature at Florida. Note the different ranges of the y-axes.

In the literature nothing about two maximum values of b, or about b-values this close to zero has been reported. From table 2.2 one can see that all exponents published in previous studies have values that lie within the range of the positive peak of b-values in figure 4.6, regardless of temperature.

By comparing the datasets of a- and b-values to the rain rate data measured by the MRR it turned out to be the hours with no, or very little precipitation, that gives the lowest a- and b-values. A way to remove these low a- and b-values, without to much loss of overall precipitation amount was needed. A threshold of the 3 h rain rates from the MRR was defined, and all corresponding values from the data set were removed. A calculation of how much of the total amount of precipitation that was lost during this procedure was done. This was repeated for different thresholds to find an optimal compromise between minimal loss of total precipitation and removal of the singular peak for $a = 1$ and the negative values of b. Removal of rain rates below 0.025 mm/3 h was finally chosen. Combined with the removal of b-values below 0.2 this leads to an overall loss in precipitation of 0.4 %. The resulting filtered data can be seen in figure 4.7 and 4.8.

Figure 4.7 is similar to figure 4.5, except that the tall bars at a value of 1 are greatly reduced for all cases. In (a) a rapid decrease from a-values of around 50 towards 600 is still evident and values larger than 200 are nearly not evident for temperatures smaller than 3 °C. For temperatures of 6 –9 °C a maxima can be seen at values around 200-300. For temperatures above 6 °C the distribution along the x-axis is more even than for the lower temperatures.

Figure 4.8 is significantly different from figure 4.5. The minor mode is per definition not evident any more and the major mode has shrinked. In (a) the peak of the distribution has been reduced from a value of around 230 to 80. The vertex of b-values moves to the right with increasing temperature, which is confirmed by the statistical analysis (see table 4.1).

In table 4.1 the average value of b and the median have the lowest b-values at the lowest temperatures, 0.68 and 0.70. The values increase with increasing temperature and reach a maximum value of 1.13 and 1.16 at a temperature above 9°. Looking at the mean and median a-values separated by temperature at Florida one can see the same pattern as for the b-values. The lowest mean and median a-values are found at temperatures below 0 °C and an increase with increasing temperature is evident. However, the maximum value of a is found at temperatures of 6 –9 °C and a small decrease is observed

when the temperature increases above 9 °C. The mean Z-R relationship for temperatures from 6 –9 °C is then $Z = 193R^{1.12}$ and for temperatures above 9 °C, $Z = 191R^{1.13}$. These two coefficients are fairly close to the Marshall and Palmer relationship, (Wilson and Brandes, 1979), and the cold front case reported by Stout and Mueller (1968) in table 2.2. However the mean exponents found here are lower than in the MP-relationship. The cold front relationship, $Z = 198R^{1.24}$, is the relation that fits this situation the best.

Table 4.1 does also contain information about how the mean and median values of a and b change with rain rate. The highest mean a-value is found at a rain rate of 8 –10 mm/3 h and has a value of 235. The mean value of a then decreases to a value of 123 at rain rates of 15 –20 mm/3 h. At even higher rain rates the value is increasing again. The median value of a has a maximum at rain rates of 6 –8 mm/3 h with a value of 219. The lowest median of a has a value of 81 and is found at rain rates of 20 –40 mm. Looking at the b-values the pattern is first increasing and then decreasing. The lowest b-values when looking both at the mean and the median are found at the highest rain rates and has values of 0.86 and 0.94. The highest b-values are found at rain rates of 6 –8 mm/3 h with values of 1.22 and 1.21. The overall mean Z-R relationship for the highest rain rates is $Z = 165R^{0.86}$ and for the rain rates with the highest mean b-value, 6 –8 mm/3 h, $Z = 218R^{1.22}$.

When separating a-and b-values according to wind, speed a distinct pattern is evident. The values are at the lowest at calm winds, and an overall mean Z-R relationship for 0 –5 m s^{-1} is $Z = 125R^{1.01}$. Increasing wind speed gives increasing mean and median values for both a and b. However the median b-value seems to stabilize at a value of 1.11 at a wind speed of 10 –15 m s^{-1} and does not increase further with increasing wind speeds. Overall mean Z-R relationship for wind speeds above 20 m s^{-1} is $Z = 227R^{1.13}$.

Separations are also done according to wind direction at Ulriken, lower block of table 4.1. Northeasterly winds give the lowest mean and median a- and b-values, with a mean overall Z-R relationship of $Z = 101R^{0.99}$. This a-value is in the lower range compared to the values found in table 2.2 and the exponent is lower than any reported value in this table. The highest mean and median relationships are found at southwesterly winds, with a mean relationship of $Z = 180R^{1.09}$ between 180 –225°.

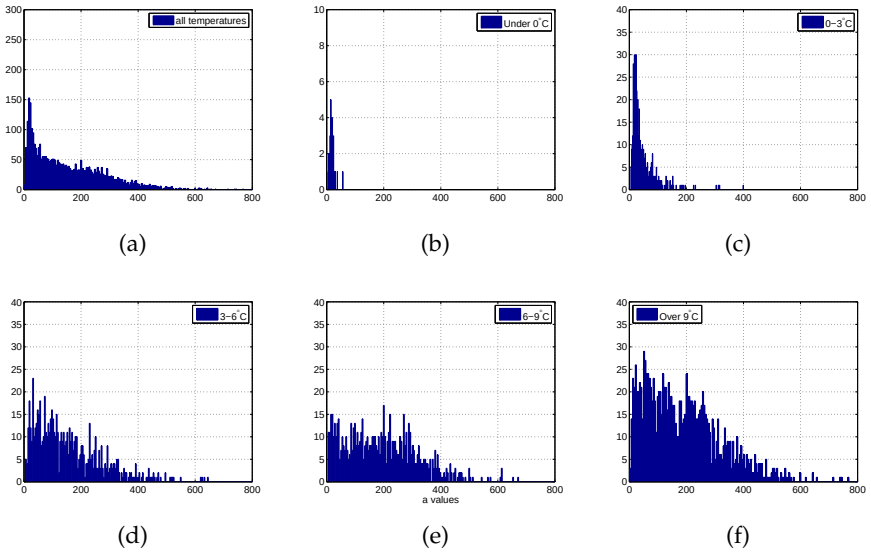

Figure 4.7: $Z = aR^b$. a-values separated by the temperature at Florida. Rain rates below 0.025 mm/3 h and b-values below 0.2 are removed. Note the different ranges of the y-axes.

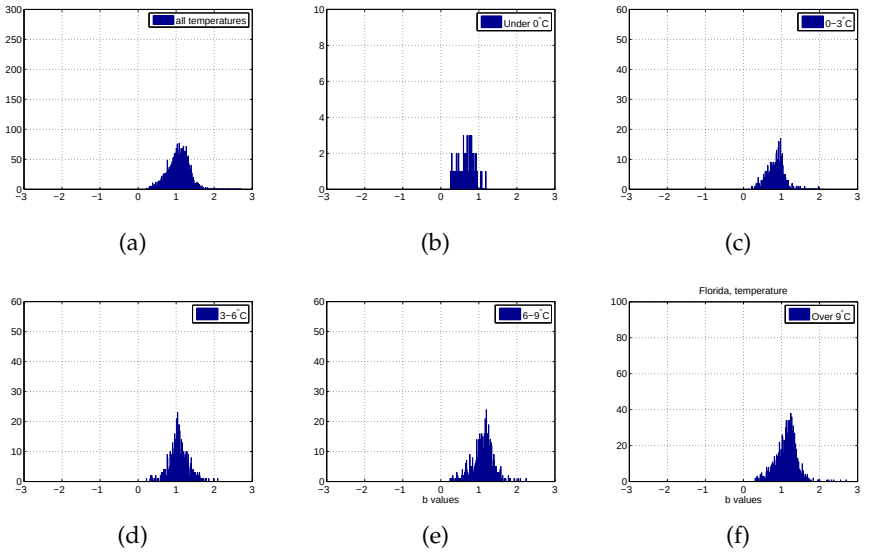

Figure 4.8: $Z = aR^b$. b-values separated by the temperature at Florida. Rain rates below 0.025 mm/3 h and b-values below 0.2 are removed. Note the different ranges of the y-axes.

	a		b	
	Mean	Median	Mean	Median
All values	158	125	1.06	1.07
under 0 °C	18	18	0.68	0.70
0 –3 °C	46	30	0.84	0.86
3 –6 °C	157	129	1.07	1.05
6 –9 °C	193	184	1.12	1.15
over 9 °C	191	169	1.13	1.16
0 –2 mm/3h	138	99	1.00	1.02
2 –4 mm/3h	192	176	1.20	1.20
4 –6 mm/3h	206	198	1.21	1.20
6 –8 mm/3h	218	219	1.22	1.21
8 –10 mm/3h	235	200	1.17	1.10
10 –15 mm/3h	183	114	1.07	1.01
15 –20 mm/3h	123	96	1.03	0.98
20 –40 mm/3h	136	81	0.92	1.00
over 40 mm/3h	165	126	0.86	0.94
0 –5 $m\,s^{-1}$	126	85	1.01	1.01
5 –10 $m\,s^{-1}$	142	109	1.05	1.06
10 –15 $m\,s^{-1}$	184	156	1.08	1.11
15 –20 $m\,s^{-1}$	195	170	1.11	1.11
over 20 $m\,s^{-1}$	227	239	1.13	1.11
0 –45°	101	51	0.99	0.98
45 –90°	167	141	1.06	1.10
90 –135°	176	163	1.08	1.12
135 –180°	130	92	0.99	0.99
180 –225°	181	153	1.09	1.12
225 –270°	174	155	1.07	1.08
270 –315°	135	112	1.03	1.04
315 –360°	115	87	1.06	1.03

Table 4.1: Average and mean values of the bars in figure 4.8 and 4.7. Temperature and rain rates are measured at Florida. Wind speed and wind direction is measured at Ulriken.

4.4 3 h rain rates after filtering of low rain rates and b-values

The removal of the lowest b-values and rain rates below 0.025 mm/3 h caused only a reduction of 0.4 % of the total precipitation amount over this three year period. This is however expected to have an effect on the statistical parameters, as the coefficients in the linear regression and the coefficients of determination. By removing a considerable number of data points at or very close to the origin and thus also close to the optimum regression, the coefficient of determination should decrease and outliers far away from the 1:1 line should get a stronger influence on the slope of the regression line. However, these new parameters will give a more realistic description of the statistics of this precipitation measurement method.

Figure 4.9 shows the 3 h rain rates from MET Norway and the MRR plotted against each other. This is the same as in figure 4.3, but now rain rates below 0.025 mm/3 h and b-values below 0.2 are removed. (a) shows the overall 3 year period, (b), (c) and (d) shows the individual years. The slopes of the best-fit equations vary between 0.83 and 0.91, and the coefficients of determination range between 0.17 and 0.48. These new slopes of the equations deviate more from the 1:1 line than in figure 4.3. The coefficients of determination are lower than before removal of low rain rates and b-values and the intersection points with the y-axes are further away from the origo.

Figure 4.10 corresponds to figure 4.4. Again the overestimation is evident for temperatures below 6 °C. The greatest overestimation is found at temperatures of 0 –3 °C where the MRR measures 2.64 mm for every 1 mm the gauge from MET Norway measures. For temperatures above 6 °C underestimation occurs. The slopes are lower than in figure 4.4 (a) and the understimation has increased from about 25 % to almost 30 %. All years behave in a similar way, but some year to year variability is evident. For example for the temperature interval between 3 –6 °C the best-fit equation overestimates the rain rate in year 2 and year 3, while an underestimation can be seen in year 1.

In table 4.2 all coefficients of determination before and after removal of low rain rates and b-values are summarized. In 18 out of 24 cases the removal of low rain rates and b-values caused the expected slight decrease in R^2, see table 4.2. In 17 out of 18 cases the intersection point with the y-axis has also moved further away from the origin.

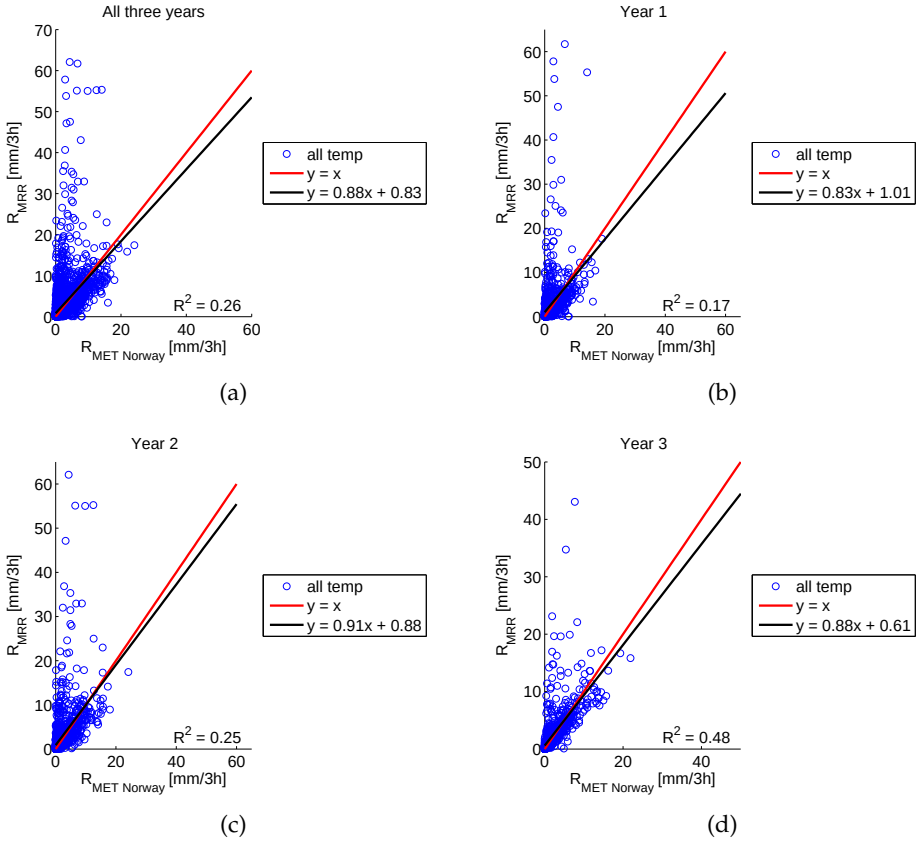

Figure 4.9: 3 h precipitation measured by MET Norway vs. precipitation measured by the MRR. Rain rates below 0.025 mm/3h and times with *b*-values below 0.2 are removed. R^2 is the coefficient of determination.

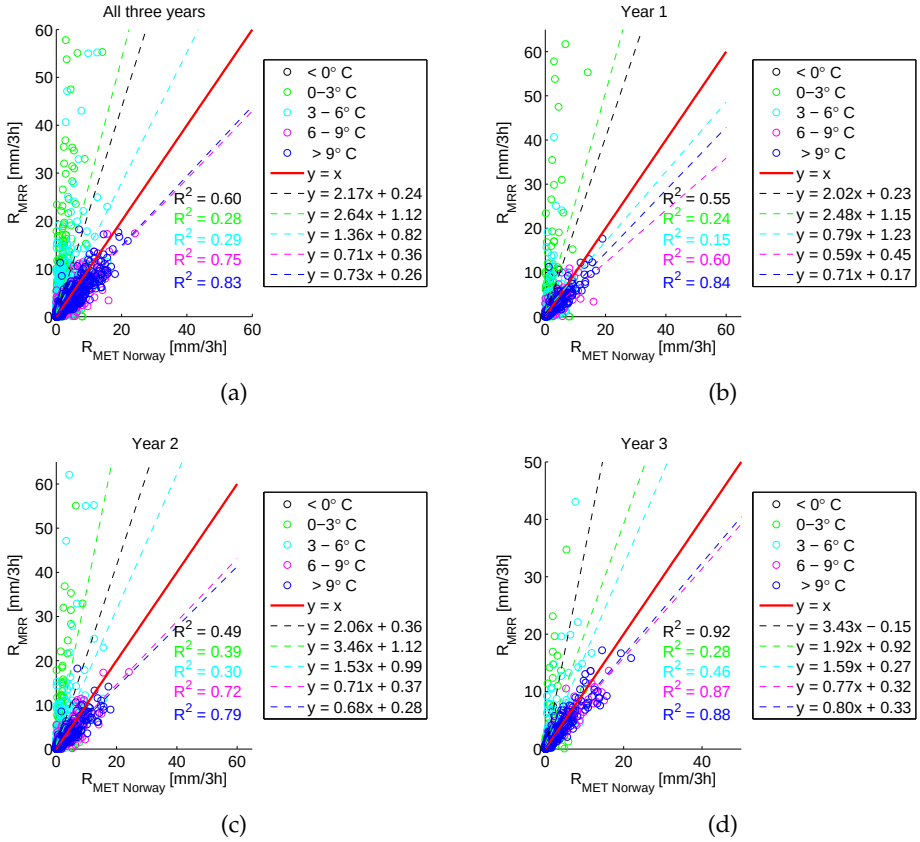

Figure 4.10: 3 h precipitation measured by MET Norway vs. precipitation measured by the MRR. Rain rates are separated by the air temperature at Florida. Rain rates below 0.025 mm/3h and times with b-values below 0.2 are removed. R^2 is the coefficient of determination.

		R^2 when all rain rates and b-values are included.	R^2 when low b-values and rain rates are removed.
all years	all temp.	0.35	0.26
	< 0 °C	0.59	0.60
	$0 - 3$ °C	0.27	0.28
	$3 - 6$ °	0.37	0.29
	$6 - 9$ °C	0.80	0.75
	> 9 °	0.87	0.83
Year 1	all temp.	0.25	0.17
	< 0 °C	0.57	0.55
	$0 - 3$ °C	0.24	0.24
	$3 - 6$ °	0.24	0.15
	$6 - 9$ °C	0.69	0.60
	> 9 °	0.88	0.84
Year 2	all temp.	0.33	0.25
	< 0 °C	0.58	0.49
	$0 - 3$ °C	0.32	0.39
	$3 - 6$ °	0.37	0.30
	$6 - 9$ °C	0.77	0.72
	> 9 °	0.84	0.79
Year 3	all temp.	0.57	0.48
	< 0 °C	0.76	0.92
	$0 - 3$ °C	0.27	0.28
	$3 - 6$ °	0.56	0.46
	$6 - 9$ °C	0.90	0.87
	> 9 °	0.90	0.88

Table 4.2: Summary of the coefficients of determination for figure 4.3, 4.4, 4.9 and 4.10.

Figure 4.11 shows the relationship between 3 h a- and b-values and rain rates for the overall three year period. The times with rain rates below 0.025 mm/3 h and b below 0.2 are removed. The top panel shows the relationship between a- and b-values. a varies between 0 and almost 1000. However, values above 600 are very rare. The vast majority of b-values are below 2. The sparse higher values of b are associated with a-values less than 200. The values of b increases rapidly for a-values below 30 and are then mostly concentrated in the band between 0.8 and 1.5 for higher values of a. Above a-values of around 200, b seems to be more or less independent of a. The panel in the middle illustrates the relationship between rain rates and a-values. No clear relationship between both parameters can be found. However, the maximum values of a seem to drop at around 15 mm/3h. It has to be taken into consideration that values exceeding 20 mm/3h most likely are influenced by overestimation due to the melting layer in the lowest range bins. In the bottom panel a rapid increase in b-values is evident for rain rates below 1 –2 mm/3h. However, larger rain rates do not seem to have a significant influence the mean values of b, but the variability clearly decreases.

Top panel in 4.12 (a) shows a nearly perfect linear relationship between a- and b-values for a-values between 5 and 20. This linear relationship is also evident for the higher temperature intervals. For a-values above 20, a and b seem to be more or less independent of each other.

The middle panel shows the relationship between rain rates measured by the MRR and a-values. For temperatures below 0 °C the value of a increases rapidly to values of around 20 for rain rates below 2 mm/3h. Increasing rain rates do not seem to affect the value of a significantly, but increasing temperatures seems to give higher a-values and a greater spread among the a-values. However, an obvious relationship between rain rates and a-values is not evident for the individual temperature intervals.

The lower panel shows the relationship between rain rates and b-values. For rain rates below 2 mm/3h a sharp increase in b-values are evident. The value of b seems to be unaffected by higher rain rates. However higher temperatures give in general higher values of b.

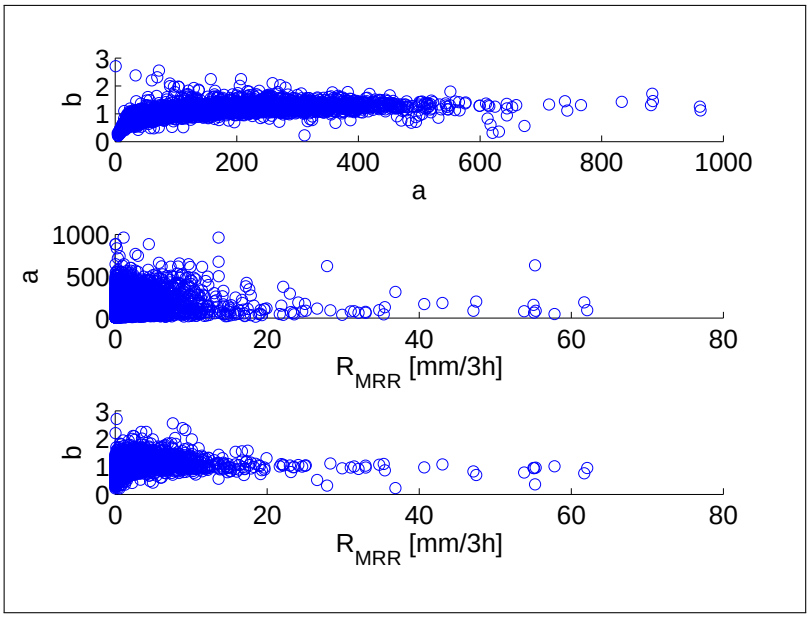

Figure 4.11: Showing the relationship between 3 h a- and b-values and rain rates from the MRR. $R_{MRR} < 0.025\,\mathrm{mm}/3\,\mathrm{h}$ and $b < 0.2$ are removed.

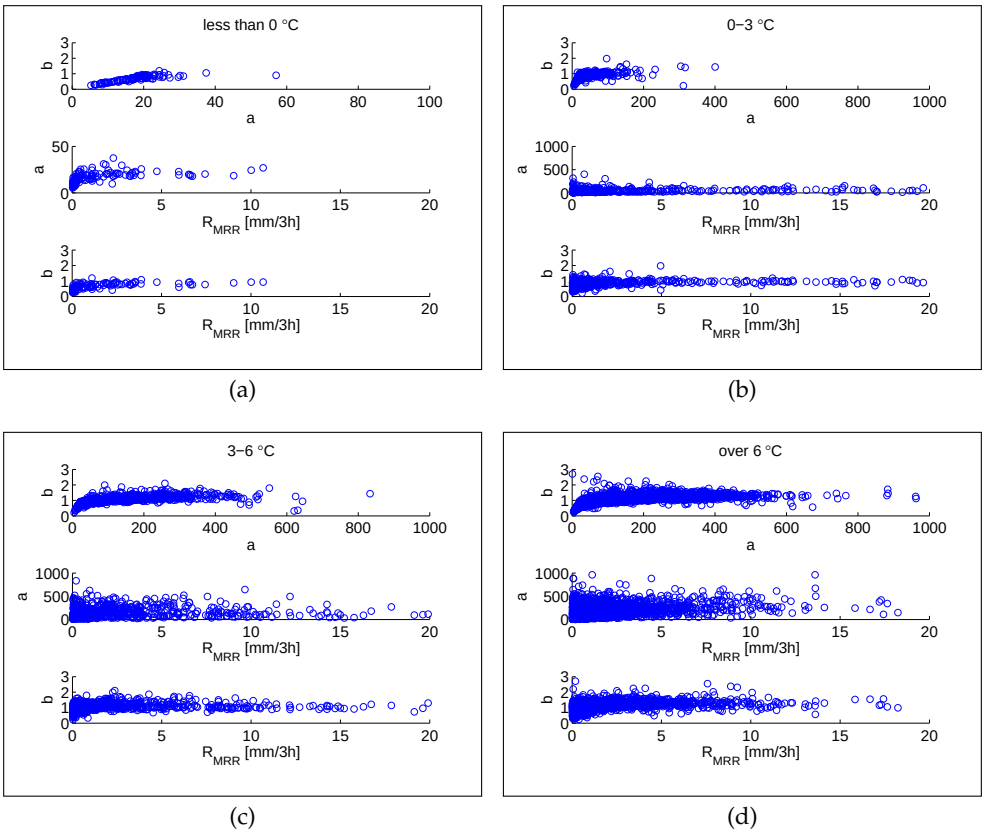

Figure 4.12: Relationship between a-values, b-values and rain rate for the overall 3 year period. $R_{MRR} < 0.025\,\mathrm{mm/3\,h}$ and $b < 0.2$ are removed and separations are due to ground temperature at Florida. Note that the top panel in (a) has a different x-axis than (b) - (d) and that the middle panel of (a) has a different y-axis than (b) - (d).

CHAPTER 5

Case studies

The MRR provides more information than just the amount of precipitation reaching the ground. It also provides vertical distribution of fall velocities and reflectivity. Indirectly it also gives information about the vertical temperature structure of the atmosphere. A sharp change in fall velocities can be seen where snow melts and transforms into rain. In a warm air mass this melting layer will be further away from the ground than in a cold air mass. In cases of ground temperature below freezing there might be no visible bright band at all.

The case studies presented in the following will investigate the changes in the vertical structure of precipitation dependent on the synoptic situation. A special focus will be given to the corresponding variation of the parameters a and b in the Z-R relationship. The following synoptic situations/time periods have been selected:

1. Quasi-stationary front, 05-06.10.2010

2. Warm air advection, 29.10.2010

3. Convective rain, 28-29.06.2011

5.1 Case 1: Quasi-stationary front , 05 - 06.10.2010

A low pressure system is in 5.1 (a) located south-west of Svalbard with a front extending down along the coast of Norway. At 0000 UTC 05.10.10 this front is moving westward and Bergen is in the warm sector of a developing frontal wave. The warm part of this front is moving northward and a cold front is slowly moving in towards Bergen. This cold front reaches Bergen a bit before 1800 UTC the first day and can be seen as a temperature decreasse of 6 °C at Ulriken and 7 °C at Florida between 1710 UTC and 2030 UTC, see figure 5.5. At this time the low pressure system that was previously located south of Svalbard has moved north and weakened. The cold front causing the temperature reduction is now merging with the occlusion of the larger low pressure system located south of Iceland. At 0000 UTC 06.10.10 the cold front is still located along the coast of Norway and the temperature is fairly constant at Ulriken until 14 UTC. The low pressure system is rotating, forcing warm air northward and cold air southward. Around noon the second day, figure 5.1 (g), Bergen is once again in the warm sector and the temperature at Ulriken increases by 1.3 °C in the course of 20 minutes starting at 1400 UTC. The system keeps rotating and pushes in a new cold front shortly before 1800 UTC. This causes a slow decrease in temperature the rest of the day.

The pressure is fairly constant from midnight the 5^{th} untill 1630 UTC with an average pressure of 991.4 hPa. Between 1630 UTC and 2100 UTC it increases by nearly 5 hPa. This is compatible with the temperature drop and the cold front along the coast of Norway in figure 5.1 (d). The pressure is then relatively constant untill 1200 UTC the next day. A pressure decrease of 5.7 hPa takes place between noon and 1650 UTC where it reaches its minimum value. The increase of pressure the rest of the day is consistent with the temperature decrease and the new cold front approaching around 1800 UTC.

The wind direction measurements at Florida indicate nearly continuous southerly channeled flow in the valley throughout this two day period with a mean value of $4.7\,\mathrm{m\,s^{-1}}$. This is around $10\,\mathrm{m\,s^{-1}}$ lower than at Ulriken. Unfortunately, the wind direction measurement at Ulriken are corrupted at that time, showing a more or less arbitrary distribution.

In figure 5.2 the melting layer, indicated by the bright band and an increase of the fall velocity of the hydrometeors, is located at an altitude of about

2600 m until noon on October 5^{th}. The precipitation is intermittent and of shower-like structure during that time. After noon the altitude of the melting layer decreases to 2300 m and retains this altitude throughout the day with only a weak increase up to 2500 m before the altitude decreases to 2300 m again between 1600 UTC and 2000 UTC. Between 1330 UTC and 2100 UTC the precipitation is nearly continuous, but with varying intensity. Something worth noting is that this slight increase in altitude virtually concides with the time when the temperature at the ground decreases rapidly, a time where it would be expected that the bright band altitude would decrease as well. At midnight the 6^{th} the bright band lies closer to the ground than the previous day and is fairly constant at an altitude of 1800 m until noon. After noon there is a slight increase in height before it subsides to 1500 m between 1800 UTC and 2000 UTC. Except for one hour around 0400 UTC there is continuous and rather intense rainfall until 2000 UTC where the precipitation stops abrupt.

Figure 5.3 and 5.4 visualize the relationship between a-values, b-values and rain rate on a hourly basis. Minute values of precipitation are shown in the middle panel of the first figure. The overall Z-R ratio for the selected period is $Z = 246R^{1.04}$ when based on the mean values of a and b. For the corresponding median values the relationship is $Z = 200R^{1.06}$, see table 5.1.

Comparing these Z-R relations to the relationships in table 2.2, one can see that b-values this low are only reported by Fujiwara (1967) for two cases in Hawaii. However, these two cases have the two lowest a-values in the table, and are thus not comparable to the mean and median a-values found here.

The top panel of the first figure shows that both the a- and b-values vary considerably. In particular the a-values indicate a wave-like pattern of 6 to 8 hour period. At first sight it looks like the a-value varies in the same manner as the precipitation rate in the middle and bottom panel. This can be weakly verified by figure 5.4 (b) where a sligth increase in a-values with increasing precipitation rate is evident. No clear pattern between a- and b-values is found in 5.4 (a), except of the occurence of the lowest b-values both for very low and very high values of a.

One significant feature can be identified around 1500 UTC on the second day. At that time the b-values drop temporarily below 0.5, while the a-values suddenly increase from around 250 to more than 600 for several hours. This shift coincides with the distinct increase in precipitation intensity, a temperature increase of 2 °C at Ulriken and around 3 °C at Florida, and a

slight rising of the bright band altitude. Looking at table 2.2 this rise in a-value from cold to warmer air was also observed by Stout and Mueller (1968). However, they did not report a drop in b-value.

One possible explanation for the observed behaviour of a and b could be the modification of the drop size distribution in the warmer air. A warmer air mass can hold more moisture than a colder air mass and more evaporation takes place in a warm environment. This would cause a drop size distribution containing less but larger droplets than before. The observed changes in a- and b-values could also be explained by a change in vertical velocity of the air mass.

	a	b
max	749.1	1.60
min	22.7	0.30
mean	246.1	1.04
median	199.9	1.06
standard deviation	175.7	0.29

Table 5.1: Variation of a- and b-values in case 1.

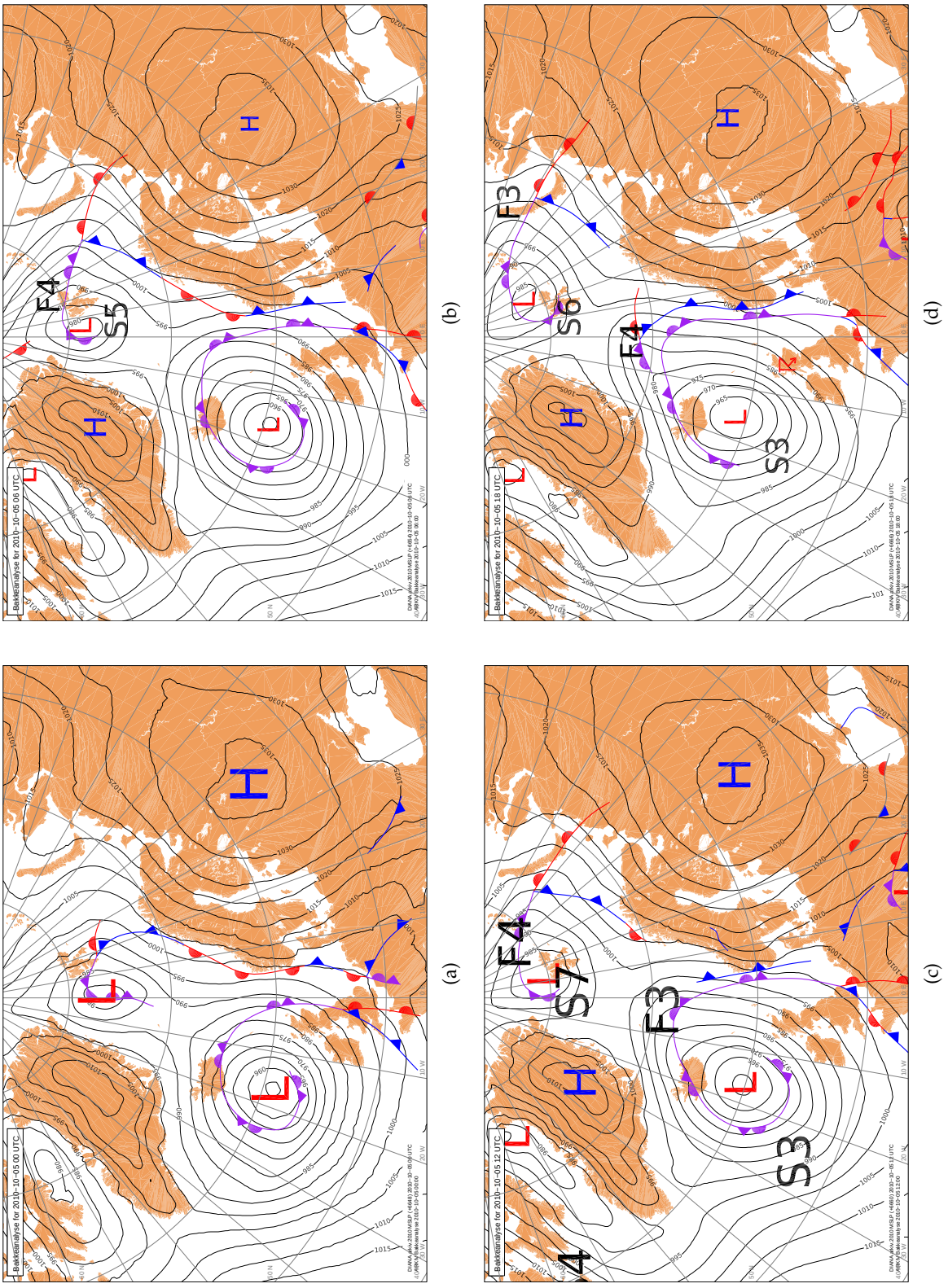

Figure 5.1: Synoptic situation 05.10.2010. (Source: Birgitte R. Furevik, MET Norway)

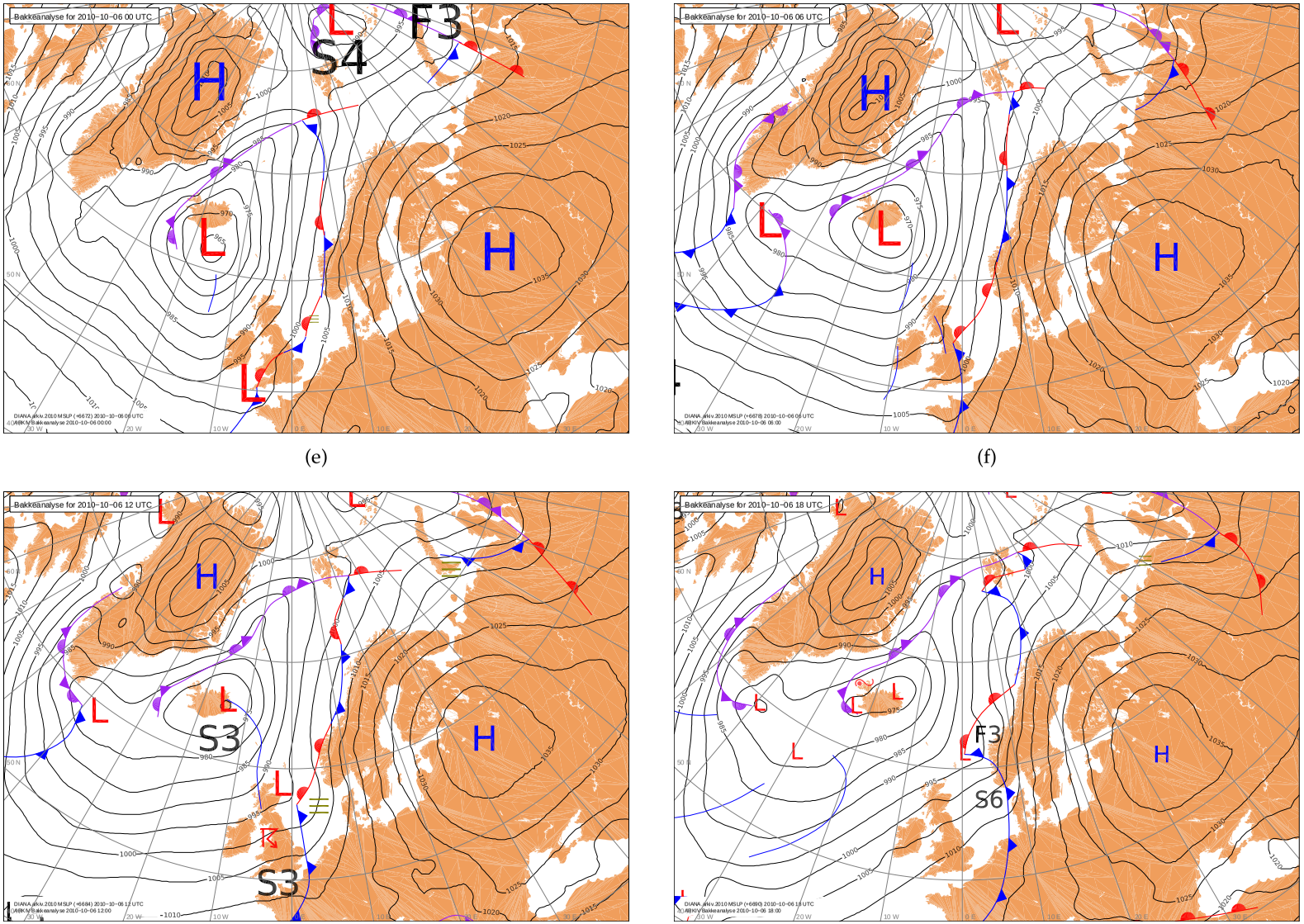

(e) (f)

(g) (h)

Figure 5.1: Synoptic situation 06.10.2010. (Source: Birgitte R. Furevik, MET Norway)

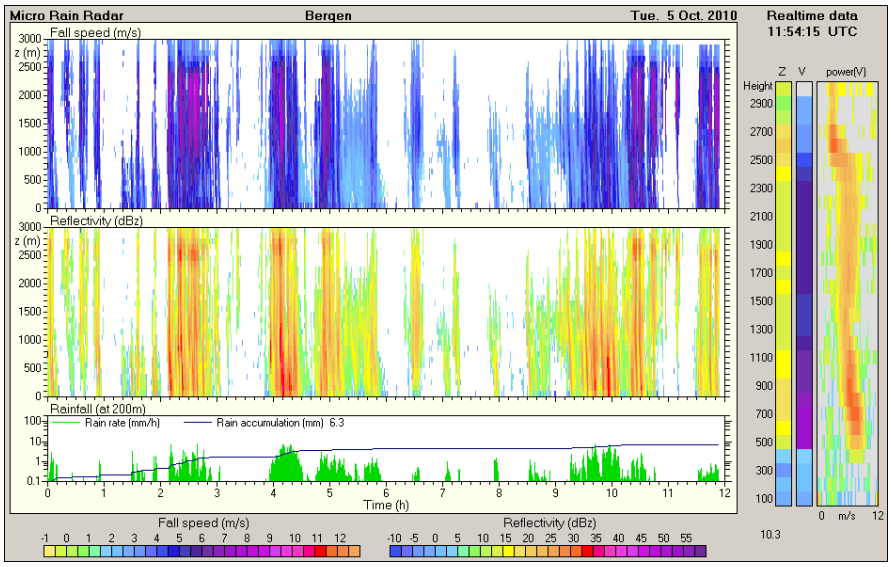

(a)

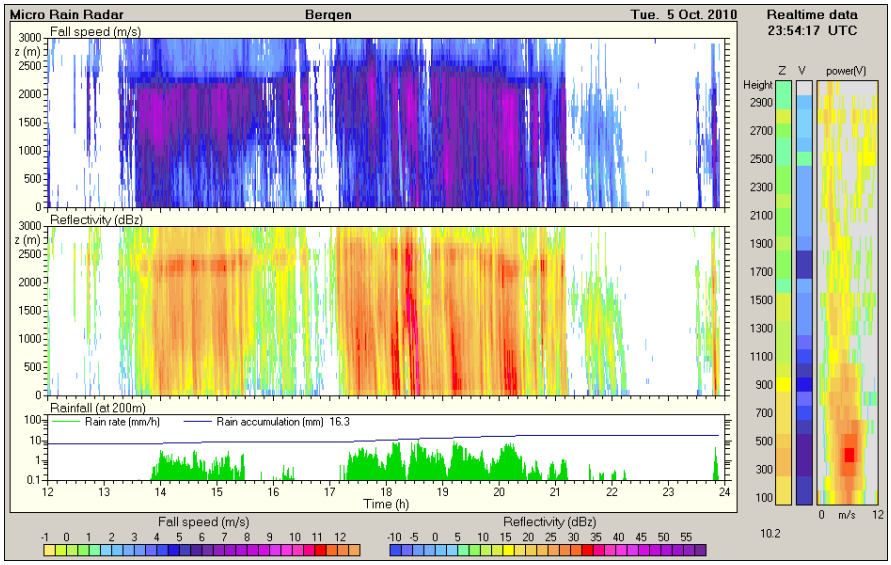

(b)

Figure 5.2: Case 1, 05.10.2011. Development of the situation, recorded by the MRR.

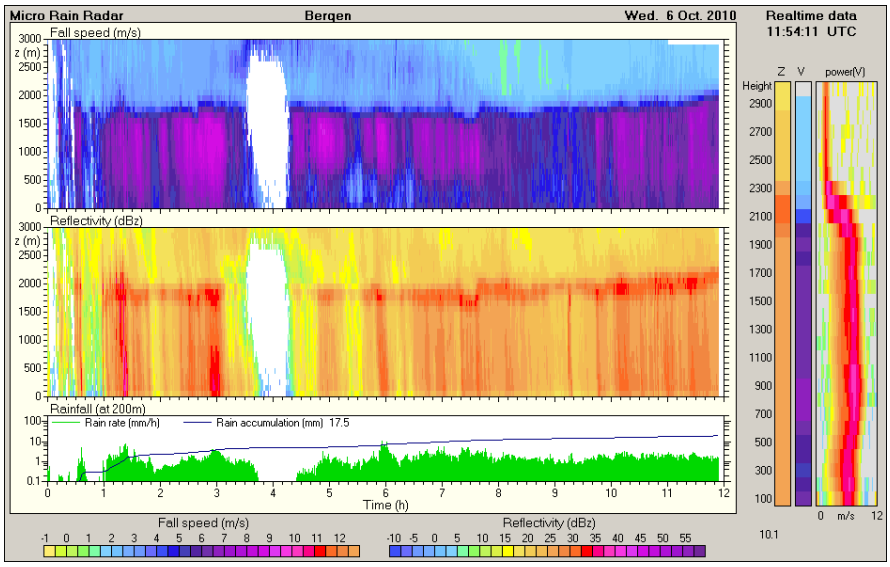

(c)

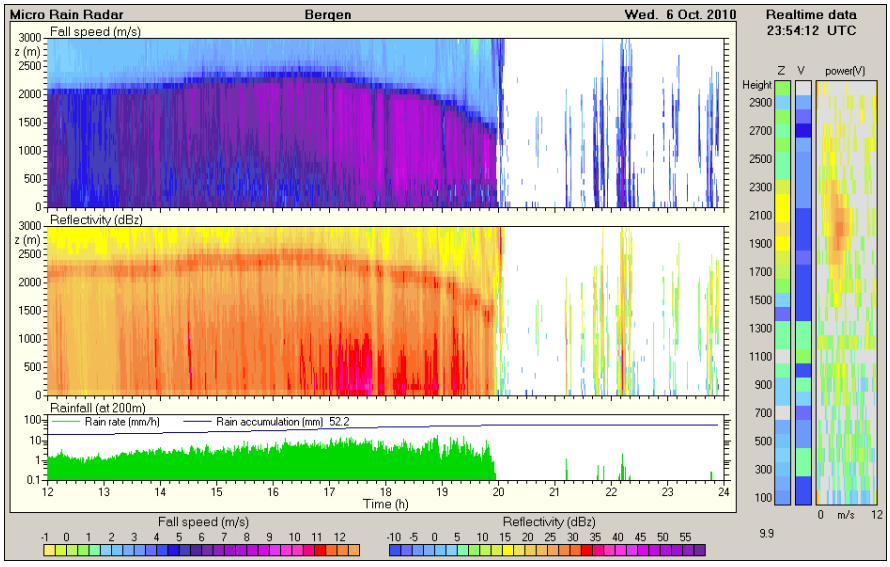

(d)

Figure 5.2: Case 1, 06.10.2011. Development of the situation, recorded by the MRR.

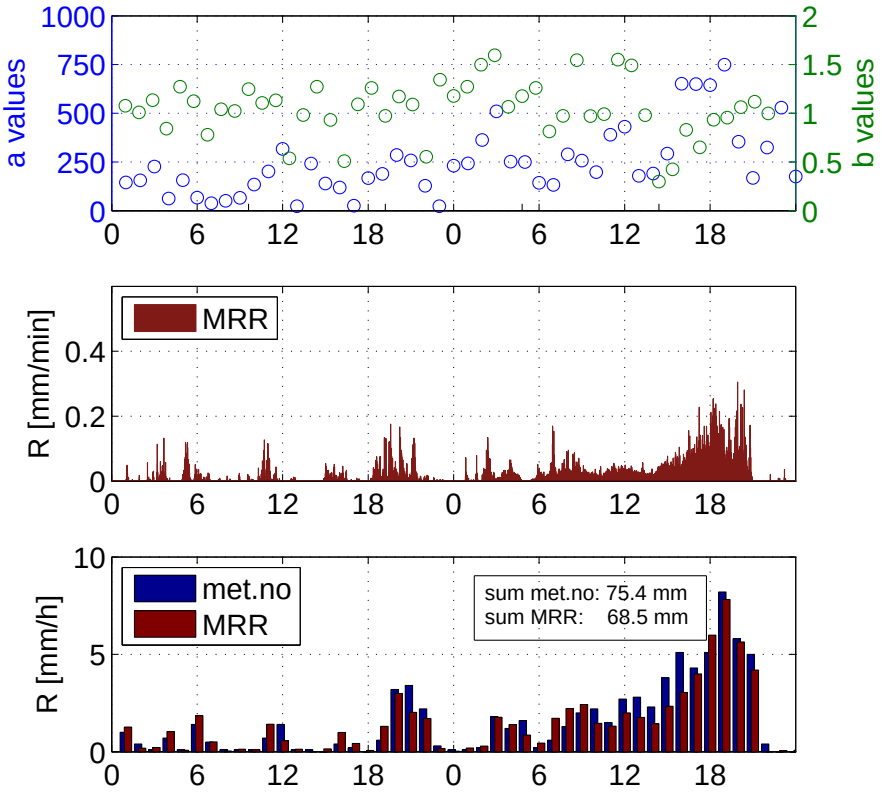

Figure 5.3: Relationship between *a*-values, *b*-values and rain rate, 05-06.10.2010. Time on x-axis.

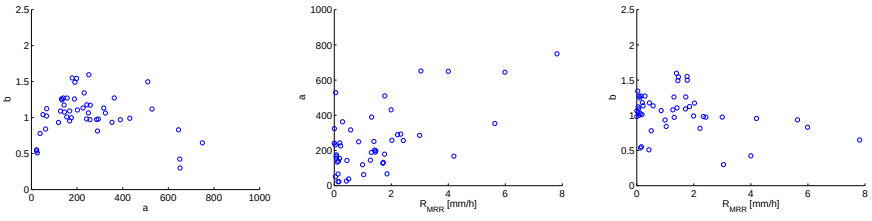

(a) (b) (c)

Figure 5.4: Relationship between *a*-values, *b*-values and rain rate, 05-06.10.2010.

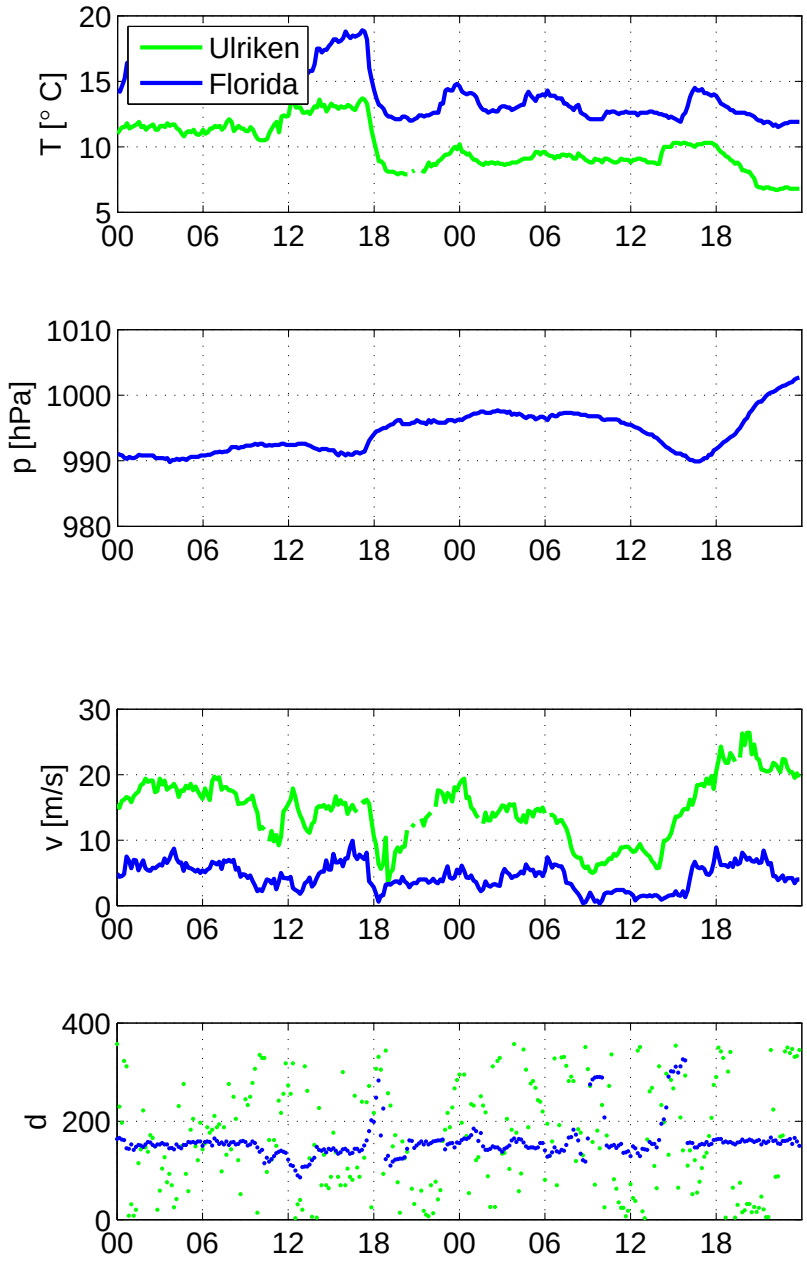

Figure 5.5: Temperature, pressure, wind speed and wind direction, 05-06.10.10. Time on x-axis.

5.2 Case 2: Warm air advection, 29.10.2010

The synoptic situation at 0000 UTC, 0600 UTC, 1200 UTC and 1800 UTC 29.10.2010 is shown in figure 5.6. A low pressure system is situated north-west of Great Britain at 0000 UTC, moving only slightly northeastward through the day. A warm front reaches the southern part of Norway at 0600 UTC and passes Bergen sometime between 0600 and 1200 UTC. A second smaller warm front is close to the west coast at 1200 UTC, moving in over the coast around 1800 UTC.

The temperature at both Florida and Ulriken increases nearly steadily through the day, but with a steeper slope from midnight to 0900 UTC than after 0900 UTC. See figure 5.10. At 0900 UTC the temperature is 5.8 °C at Ulriken and 10.5 °C at Florida. At 2010 UTC the temperatures at both locations have increased further with 1 °C. A decrese of 1.5 °C takes place at Florida and 1 °C reduction at Ulriken between 2010 UTC and 2200 UTC. The two last hours of the day the temperature increases with the steepest slope of the day. The pressure falls rather fast until 0900 UTC. The total pressure drop over 24 h is 17 hPa. The flattening of both temperature and pressure at 0900 UTC is consistent with the warm front moving over Bergen between figure 5.6 (b) and (c).

Looking at the panel showing the wind speed in figure 5.10 we have an increase of windspeed at Ulriken in the morning until 0900 UTC, and a second rise after 2100 UTC. This is in accordance to the two warm fronts moving over the west coast of Norway. Wind direction at Ulriken is fairly constant through the day, at most times south/southwesterly, but with a smaller part form south-east. At all times varying only between 160 °and 224 °. At Florida we have a nearly continuous southerly channeled flow throughouth the day with a mean value of 5.7 $\mathrm{m\,s^{-1}}$.

Figure 5.7 shows the MRR recordings from 29.10.2010. During that day the melting layer increases in two steps. In the first the altitude changes from a height of 1000 m at 0400 UTC to a height of 1400 m within one hour. The altitude of the melting layer is then constant for a couple of hours before it rises to a height of 2000 m from 0800 UTC to 0900 UTC. Precipitation starts slightly before 0400 UTC in the morning and it rains more or less continuously until 1500 UTC. After this the rain continues as showers. An interesting thing to note in figure 5.7 is that the two markant increases in

bright band height, which are indicators of a warmer atmosphere, are not evident in the measurements of temperature at Florida or at Ulriken where the temperature rises more or less continuously over a larger time period. This shows the added value of the MRR data in interpreting the synoptic situation.

In table 5.2 the overall Z-R ratios for the selected period are $Z = 174R^{0.94}$ when based on the mean values of a and b and $Z = 181R^{1.12}$ for the corresponding median values. These combinations of a- and b-values are not found in table 2.2, but the median b-value is comparable to the values found by Fujiwara (1967) for Hawaii. The a-values are fairly close to the widespread rain situation in Switzerland, 26.05.69 (Waldvogel, 1974), and the stratiform rain situation in Singapore, 09.01.98 (Kumar et al., 2011).

Figure 5.8 shows the same sort of wave pattern among a- and b-values as in case 1. Slightly before 1100 UTC the rain intensity is quite strong. This rapid change in rain intensity does not seem to have any effect on the a- or b-value at the time. However, when the intensity decreases after 1100 UTC the a-value increases and the b-value decreases. The increase in melting layer altitude in figure 5.7 between 0400 UTC and 0500 UTC corresponds to an increase of both a- and b-values. The increase in altitude between 0800 UTC and 0900 UTC does not impact the value of a, although the value of b increases. At 1500, UTC when the precipitation goes from continuous to showers the values of a and b decrease.

However, looking at figure 5.9 (a) - (c) no clear pattern of relationships between a- and b-values, a-values and rain rates, or b-values and rain rates are evident.

	a	b
max	501	1.65
min	1	-0.39
mean	174	0.94
median	181	1.12
standard deviation	140	0.64

Table 5.2: Variation of a- and b-values in case 2.

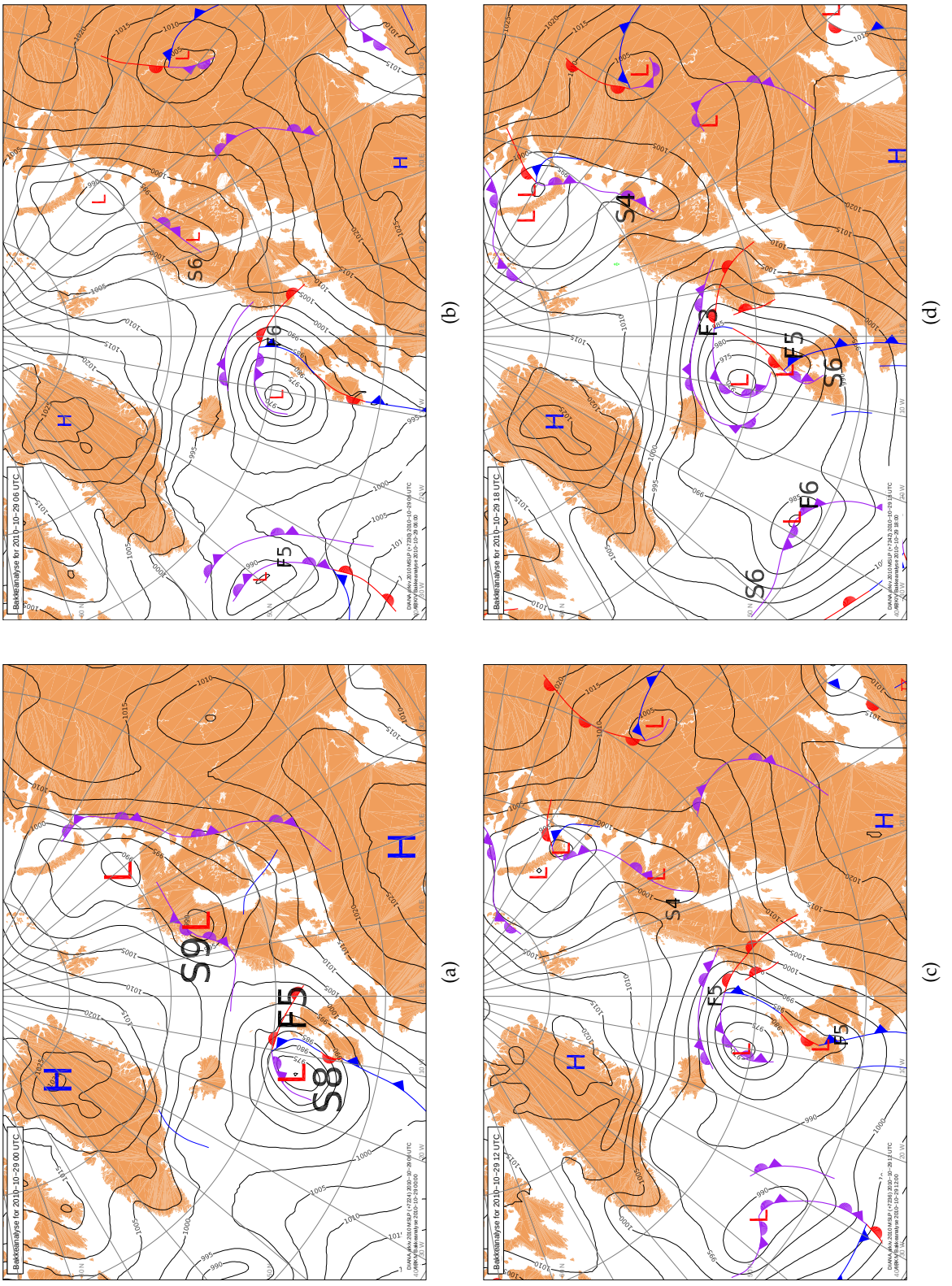

Figure 5.6: Synoptic situation 29.10.2010. (Source: Birgitte R. Furevik, MET Norway)

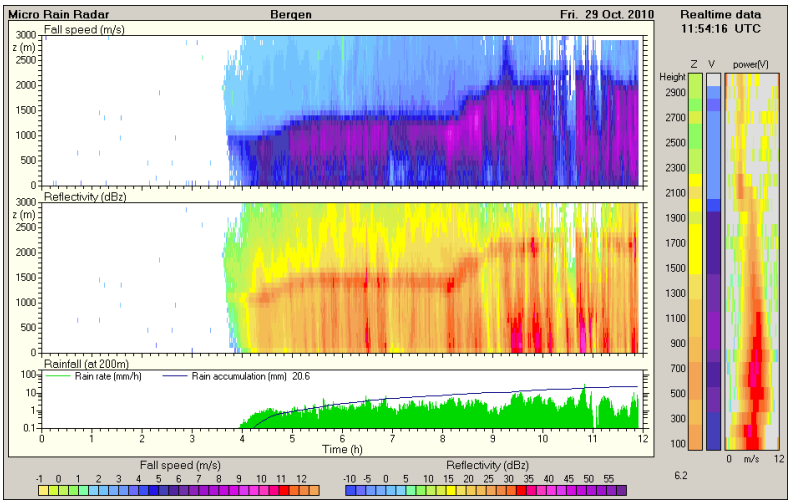

(a)

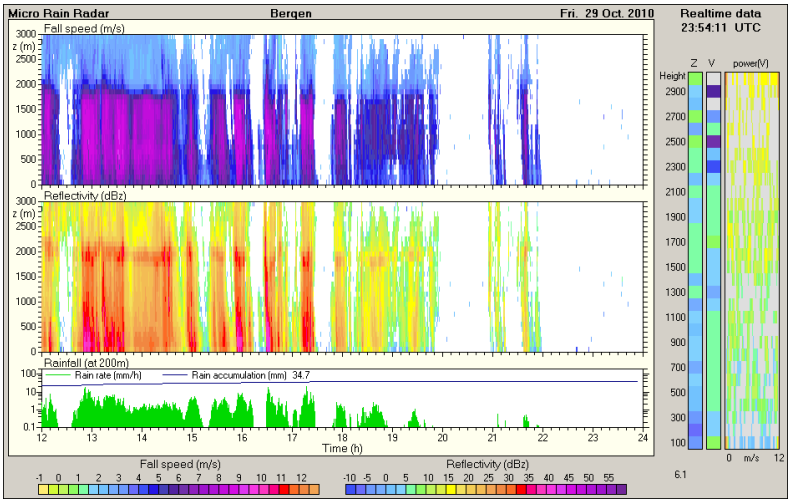

(b)

Figure 5.7: Case 2, 29.10.2010. Development of the situation, recorded by the MRR.

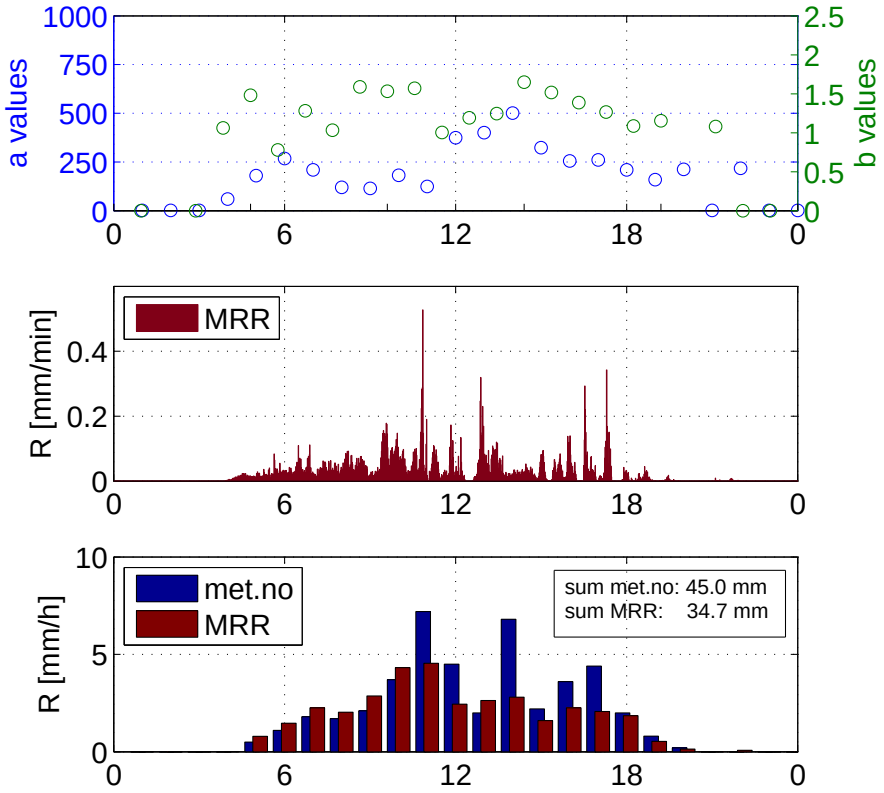

Figure 5.8: Relationship between *a*-values, *b*-values and rain rate, 29.10.2010. Time on x-axis.

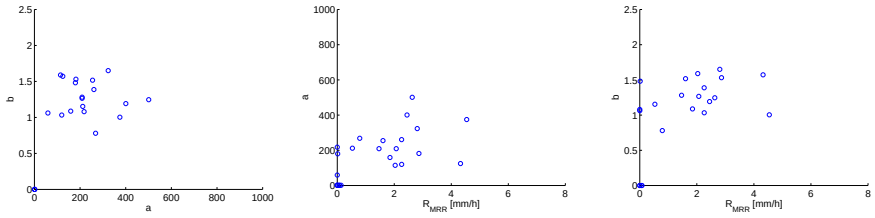

Figure 5.9: Relationship between *a*-values, *b*-values and rain rate, 29.10.2010.

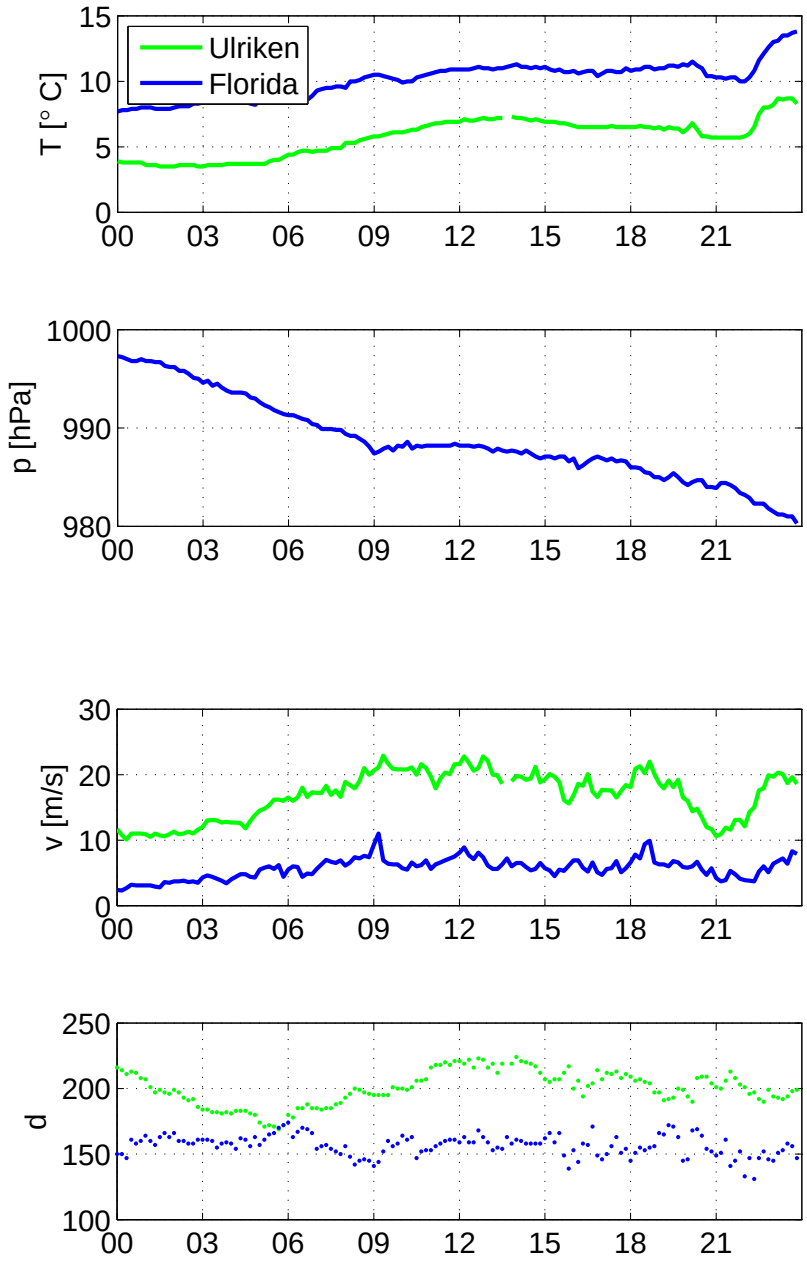

Figure 5.10: Temperature, pressure, wind speed and wind direction, 29.10.2010. Time on x-axis.

5.3 Case 3: Convective rain, 28-29.06.2011

Figure 5.11 shows how the synoptic situation develops from 0000 UTC 28.06.2011 until 1800 UTC 29.06.11. The situation is rather static, with a low pressure center located to the southeast of Iceland through the entire 48 h period. The core pressure of the system slowly increases from 1000 hPa to 1010 hPa within the two days. On the first day at 0000 UTC, a front is situated between the west coast of Norway and the east coast of Great Britain, moving slowly eastwards as time passes. Due to the rotation of the cyclone warm air is being pushed north to the east of the front and cold air southwards to the west of the front. The front moves slowly eastward and reaches the Norwegian coast between 0600 UTC and 1200 UTC on 28.06.11. Subsequently the frontal region remains nearly stationary along the coast.

Comparing maps of the synoptic situation to figure 5.15 it can be seen that the temperature at Florida and Ulriken decreases by almost 10 °C over the 48 h period. The graph showing the pressure has a wave pattern with two maxima and two minima. The first maxima occurs at June 28^{th}, 1540 UTC, with a pressure of 1011.5 hPa. The second maxima occurs right before midnight on June 29^{th}, with a pressure of 1012.3 hPa. Minimum values occurs at 0400 UTC the first day and around 0700 UTC the second day, with pressures of 1005.1 hPa and 1005.9 hPa respectively. The first pressure increase coincides with the passage of the cold front between figure 5.11 (b) and (c). The second is most likely a result of the anticyclone located over the Baltic Sea, (f).

Wind speed at Ulriken is fairly variable, but with a decreasing trend over the period. A maximum value of 21.8 $m\,s^{-1}$ occurs at 0100 UTC the first night, and a minimum value of 0.9 $m\,s^{-1}$ at noon the second day. After noon on June 29^{th} the wind speed increases slowly until midnight. The first 36 h the wind is south/southwesterly at Ulriken, but turns completely the last 12 h to north/northeasterly due to a cyclone moving eastward. In the hours before and around noon the isobars are far apart, giving the low wind speed at Ulriken, with an average of 2.0 $m\,s^{-1}$ between 1000 UTC and 1300 UTC. The wind direction at Florida is southerly until 1800 UTC the first day and northerly the rest of the period, except for a few hours around 0600 UTC on June 29^{th} where the wind is once again southerly.

Figure 5.12 shows a summer situation where the melting layer altitude

lies above 2500 m until 1000 UTC on June 29^{th}. Over the next 7 hours it decreases to an altitude of 2000 m, indicating cold air advection. During this cooling it rains nearly continuously, but with varying intensity. In general the precipitation during the 48 h period is shower-like with an additional period of continuous, but variable rain between 0000 UTC and 0430 UTC on 29.06.11. According to the MRR a total of 21.2 mm fell the first day and 31.9 mm the second day, a total of 53.1 mm over 48 hours. This is 20.5 mm less than The Meteorological Institute recorded for the same period, see figure 5.13.

Figure 5.13 and table 5.3 shows the variation among a- and b-values. The overall Z-R ratios for the selected period are $Z = 190R^{1.05}$ when based on the mean values of a and b and $Z = 188R^{1.15}$ for the corresponding median values. Both the a- and b-values are in the lower range of the values found in table 2.2. However, the a-values in this case are fairly close to the widely used Z-R relationship found by Marshall and Palmer (Wilson and Brandes, 1979), table 2.2, but the b-value is lower in this case than in the MP-relation. The relationship found by Stout and Mueller (1968), $Z = 198R^{1.24}$, for a cold front in Florida, USA, fits this convective situation the best.

A wave-like pattern among a- and b-values can be seen in figure 5.13 and it looks as if increasing rain rates gives both increasing a- and b-values. Figure 5.14 (b) and (c) confirms this and shows a weak tendency of increasing a- and b-values with increasing rain rate. Figure 5.14 (a) shows a rapid increase in b for small values of a and more or less constant values of b between 1 and 1.5 for a less than 300. This is similar to the shape of figure 4.11, top panel, where all a- and b-values for the whole three year period are plotted. However, the decreasing values of b in figure 5.14 for a-values above 300 are not evident in the three year plot.

Of particular interest is the behaviour of a- and b-values during the cooling episode on 29.06.11 from 1000 UTC to 1700 UTC. Around 1000 UTC the value of b is at a maximum of 2.3, while the value of a is at a minimum of 37. A cold front is located in the area at that time, leading to a temperature decrease of 3 °C around 0900 UTC at Florida and a 2 °C decrease at Ulriken around 1230 UTC. The a-values increase continuously from the minimum to 282 during this period, while the b-values are falling from 2.3 to 0.8.

Comparing this cold air advection situation to the weak warm air advection at 1500 UTC in case 1, section 5.1, one can see that the value of b behaves opposite in these two situations. The b-value is decreasing in the

cold air advection situation and increasing in the warm air situation. The a-value increases at the beginning of the warming period and then keeps constant for a few hours. For the cold air advection situation the a-value is increasing over the whole period. However there is no clear conclusion that the relationship between a and b is the opposite in cold vs. warm air advection situations. The observed change in a- and b-values from warmer to colder air could again be the result of a changing drop size distribution in cold air and due to a potential change in vertical velocity of the air.

	a	b
max	646	2.26
min	1	-0.18
mean	190	1.05
median	188	1.15
standard deviation	161	0.55

Table 5.3: Variation of a- and b-values in case 3.

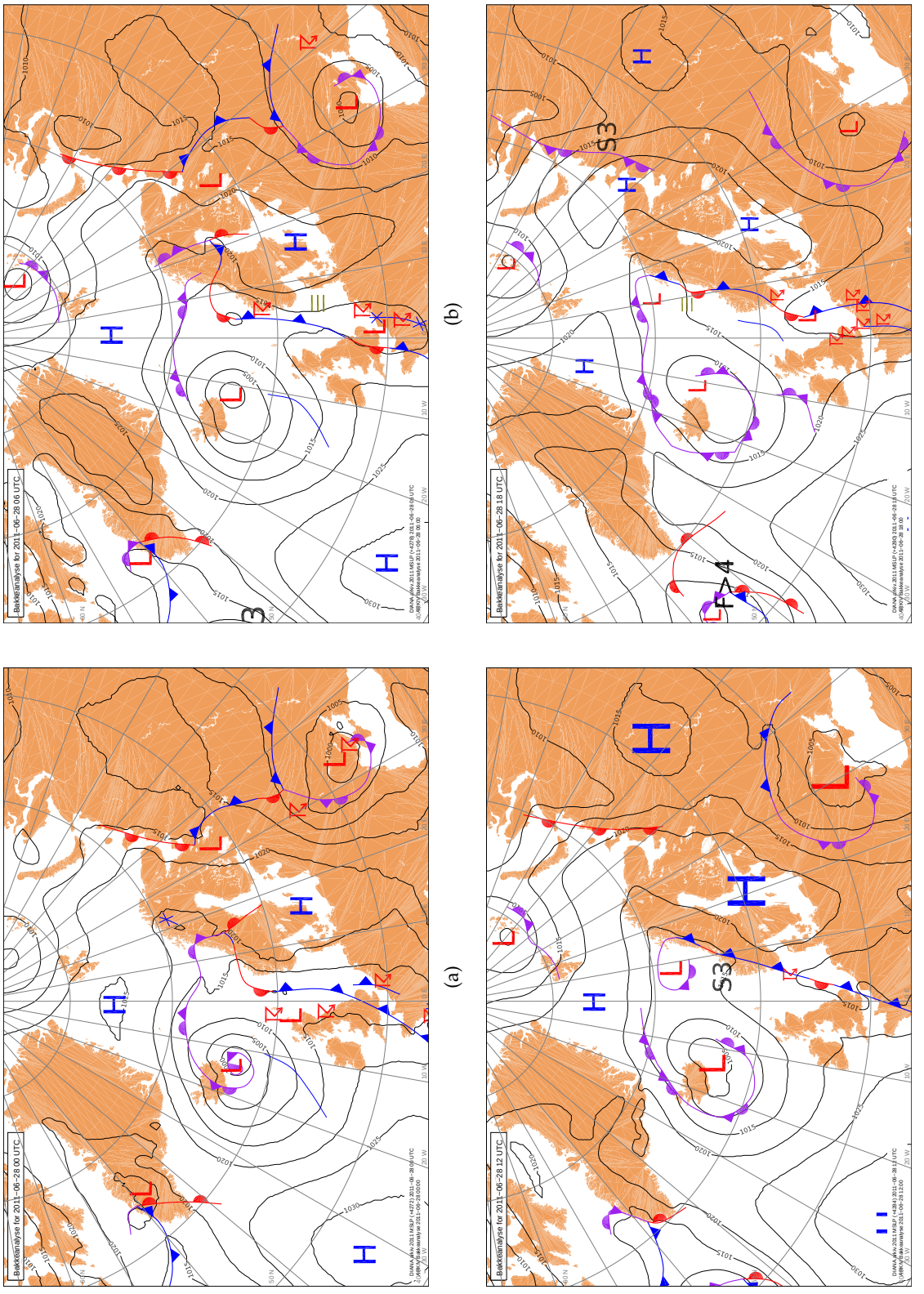

Figure 5.11: Synoptic situation 28.06.2011. (Source: Birgitte R. Furevik, MET Norway)

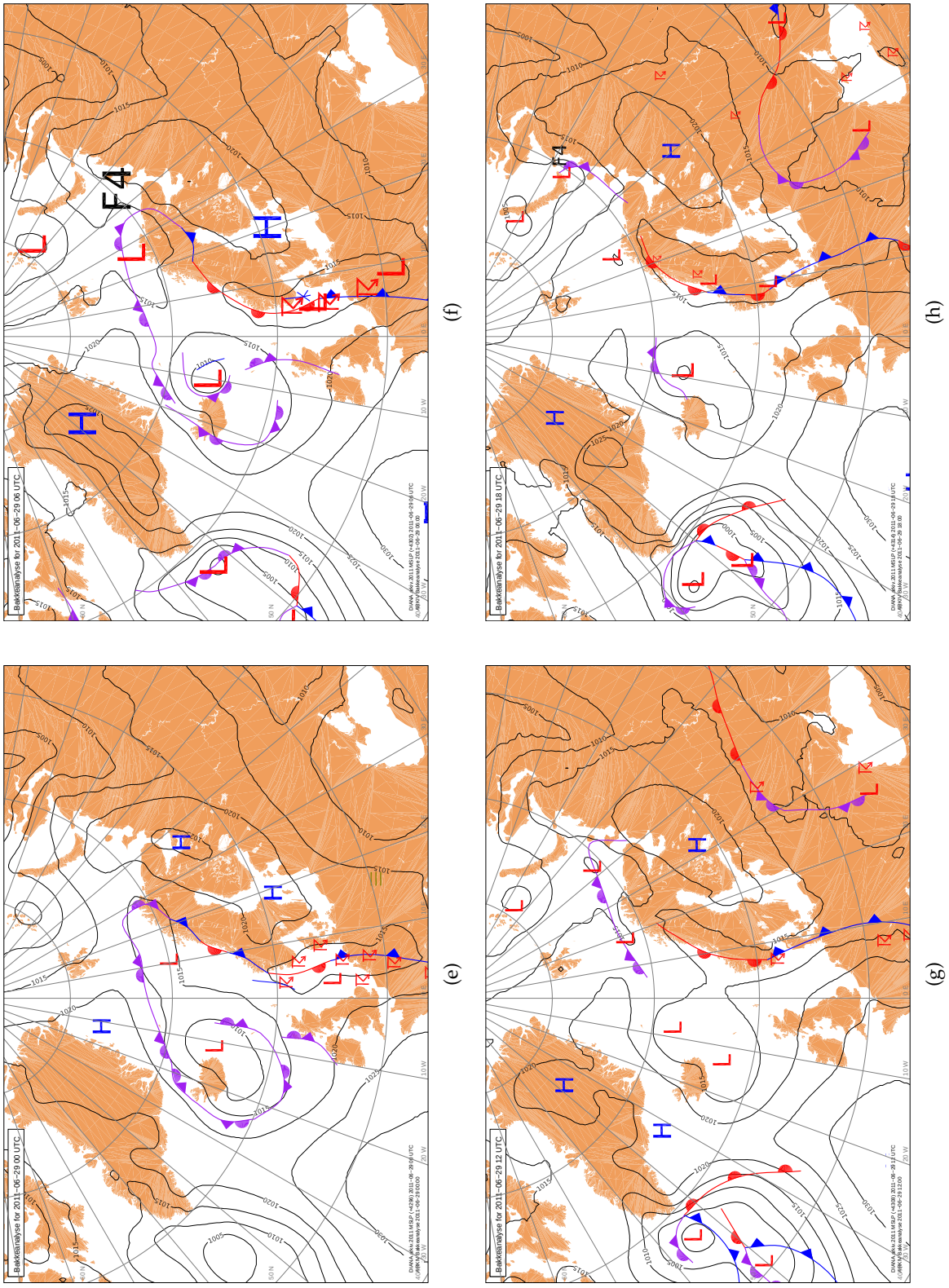

Figure 5.11: Synoptic situation 29.06.2011. (Source: Birgitte R. Furevik, MET Norway)

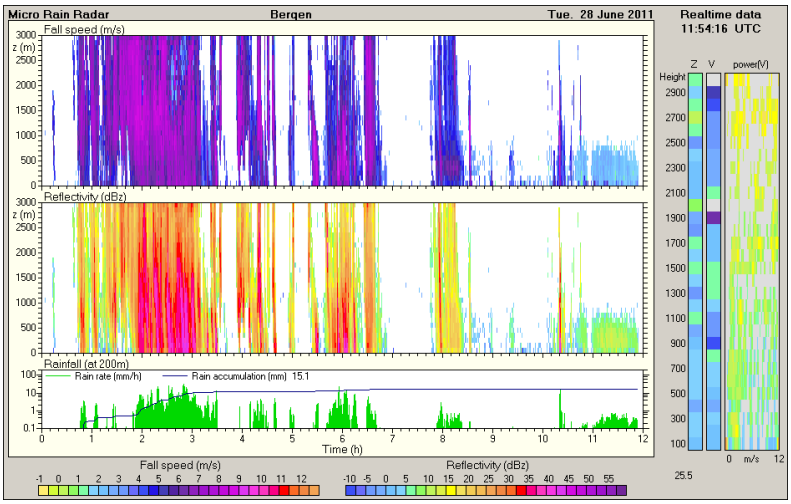

(a)

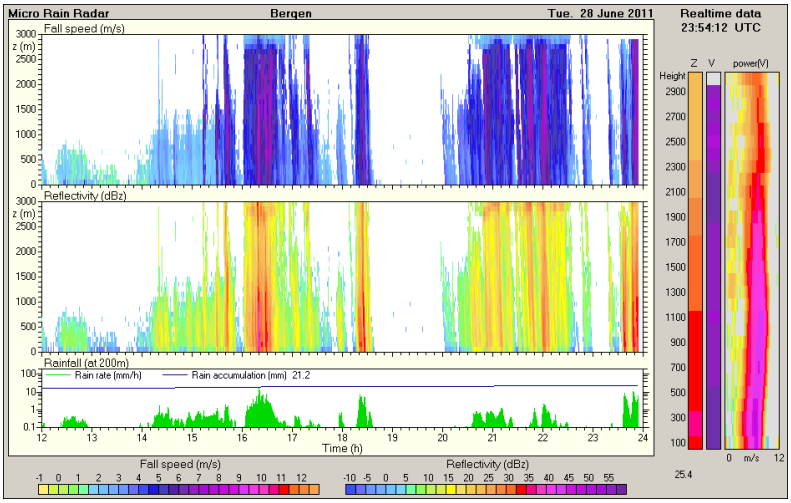

(b)

Figure 5.12: Case 3, 28.06.2011. Development of the situation, recorded by the MRR.

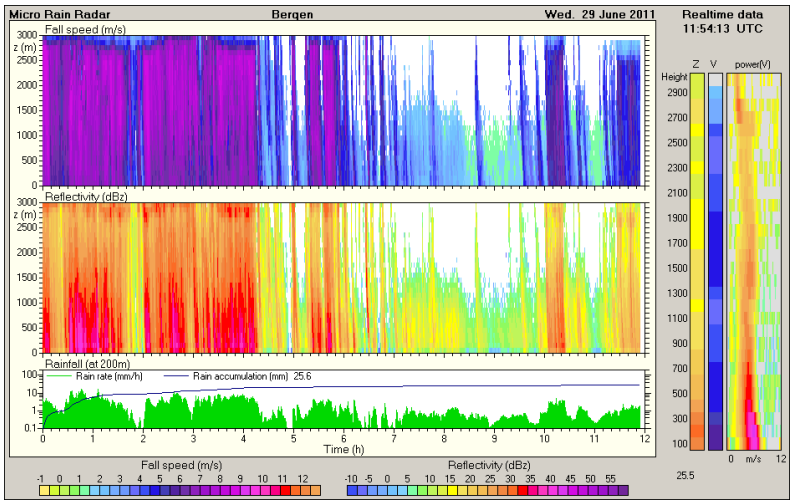

(c)

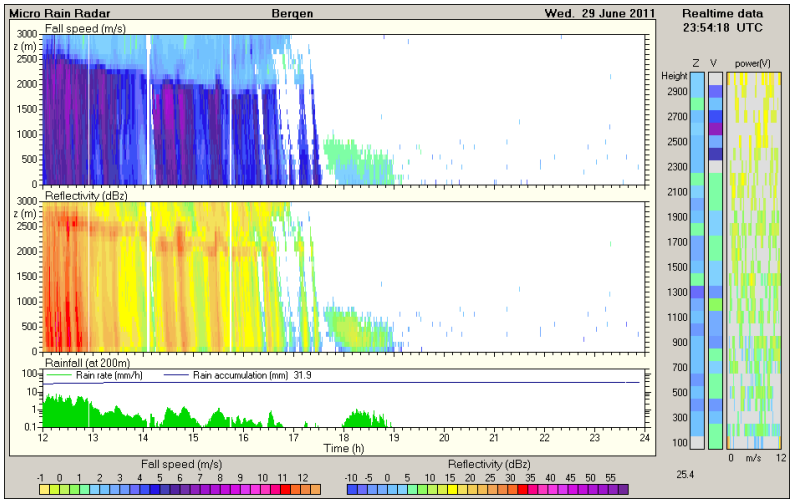

(d)

Figure 5.12: Case 3, 29.06.2011. Development of the situation, recorded by the MRR.

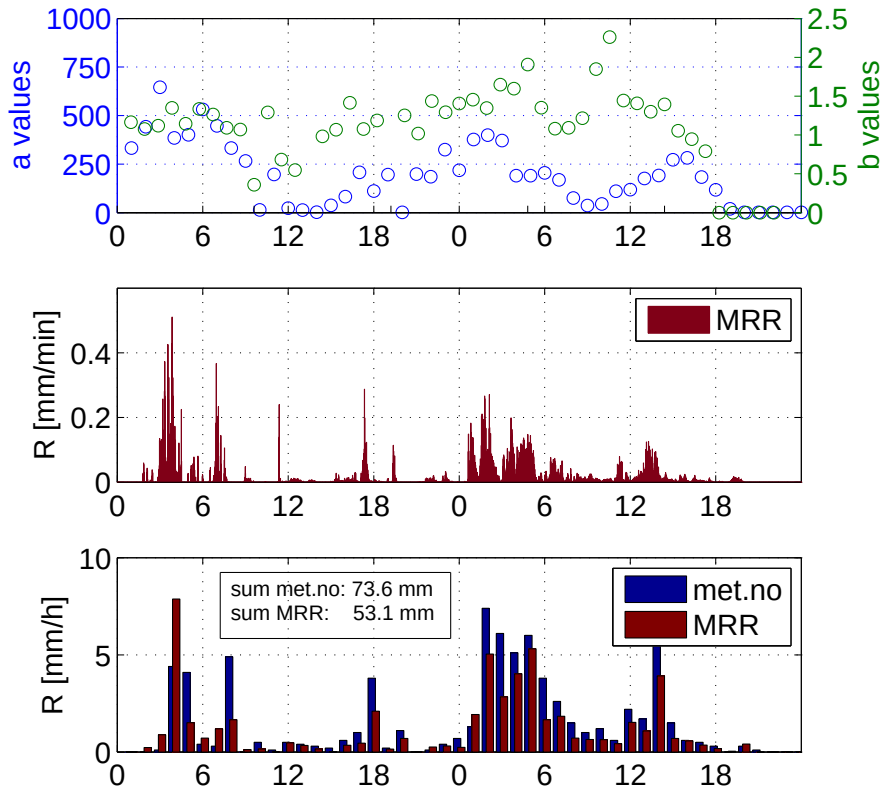

Figure 5.13: Relationship between a-values, b-values and rain rate, 28-29.06.2011. Time on x-axis.

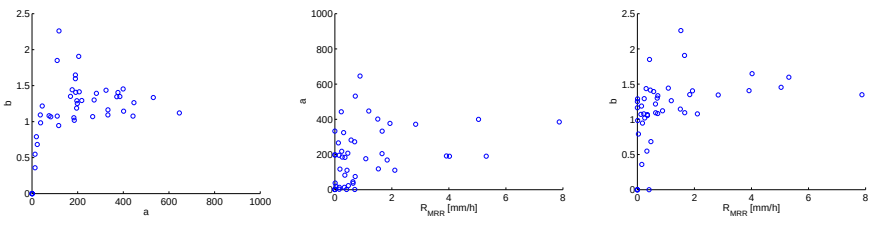

Figure 5.14: Relationship between a-values, b-values and rain rate, 28-29.06.2011.

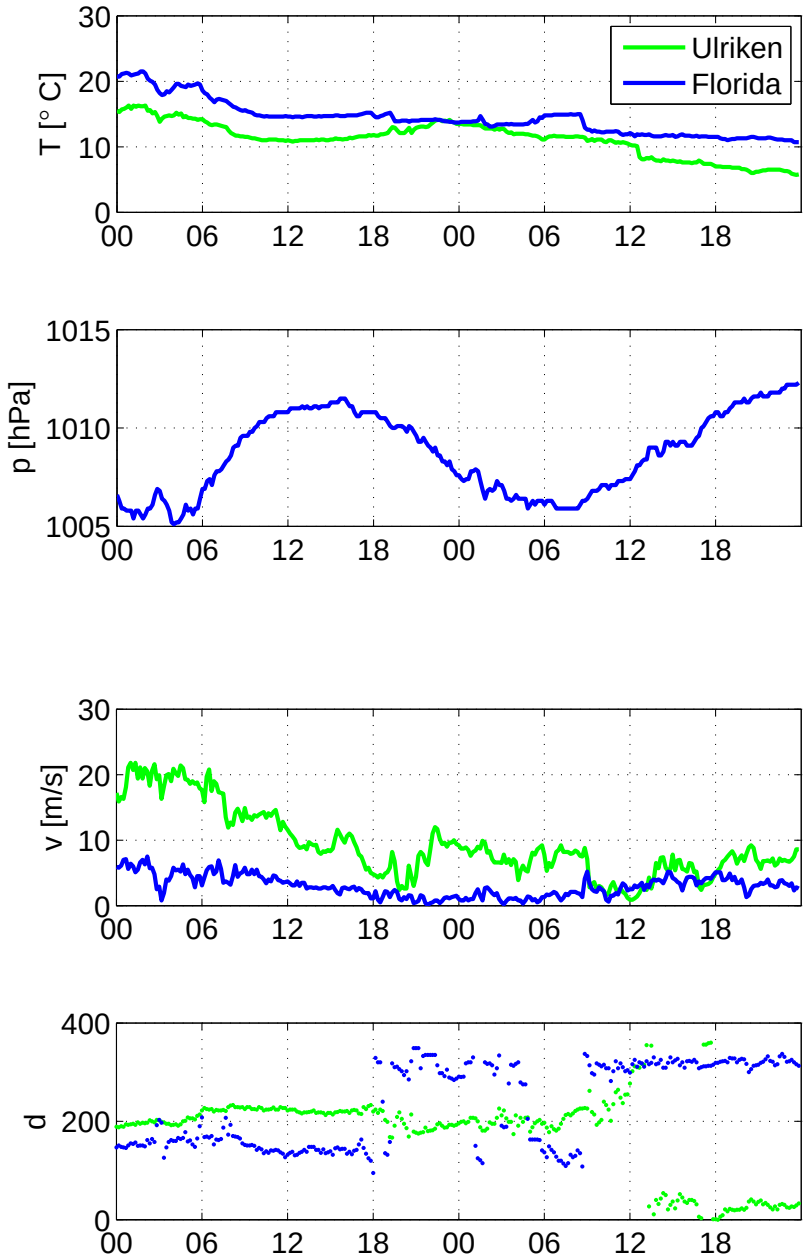

Figure 5.15: Temperature, pressure, wind speed and wind direction, 28-29.06.2011. Time on x-axis.

CHAPTER 6

Summary and outlook

In this thesis three years of precipitation measurements by the Micro Rain Radar (MRR), located at the rooftop of Geophysical Institute, have been analyzed and compared to the rain gauge measurements from MET Norway at Florida, Bergen. The measurement period started at 13.04.2010 and ended at 12.04.2013.

A comparison of the raw data of both measurement systems for annual accumulated precipitation showed an average overestimation by the MRR of 17 %. This overestimation was caused by a strong overestimation of precipitation by the MRR during the winter season with frequent occurrence of the melting layer in the lowest range bins of the MRR. During the warm season the MRR was found to underestimate the precipitation amount. A more detailed investigation on the basis of 3 h rain rates separated by temperature intervals for the station at Florida enabled a more quantitative description of the performance of the MRR system.

For the overall 3 year period the overestimation of precipitation by the MRR is largest for the temperature interval of 0 –3 °C, where it overestimates by a factor of 2-2.5. At temperatures below freezing less overestimation occurs. For temperatures above 6 °C, precipitation is underestimated by around 25 % - 30 %. Some year to year variability is evident, but in general all years behave in a similar way.

The coefficients of determination based on the linear regression are generally lowest for the temperature interval of 0 –3 °C, and increases with both increasing and decreasing temperatures. A low coefficient of determination indicates a high variability among the precipitation measurements. It is the lowest in the temperature interval of 0 –3 °C. At this temperature we are most likely to find the bright band in the range bin where the MRR estimates the rain rate, and it is in this region the highest probability of wet, water covered snowflakes occur.

Based on the one minute values of reflectivity, Z, and rain rate, R, from the MRR, the coefficients a and b of the Z-R relationship in the form $Z = aR^b$ have been calculated as 1 h and 3 h average values for further investigation. An analysis of the histograms of b showed a clear bimodal distribution with one peak for possitive and one peak for negative values of b.

A data filtering routine for the removal of times with little or no precipitation based on threshold values of the MRR rain rate and the value of b has been developed and applied. The selection of R less than 0.025 mm/3h and b less than 0.2 provided the best results by only neglecting 0.4 % of the overall precipitation amount.

After removal of low rain rates and the lowest b-values the coefficients of determination of the linear regression showed, as expected, a slight decrease. This can be explained by the fact that in the first figures (4.3 and 4.4) all data points with no precipitation are included. This is a situation where the MRR and the gauge from MET Norway generally agree as those data points are located at the origin, at the very bottom of the 1:1 line. This gives higher coefficients of determination.

In general the values of a and b are highly variable. For the overall three year period the a-values vary between 0 and 1000 and the b-values vary mainly between 0 and 2. The sparse higher values of b are associated with a-values less than 200. The b-values increased rapidly for a-values below 30 and were then mostly concentrated in the band between 0.8 and 1.5 for higher values of a. No clear relationship could be found between a-values and rain rates. The values of b increased rapidly for rain rates below 1 –2 mm/3h. Larger rain rates did not influence the mean values of b, but the variability clearly decreased.

By separating the overall relationship between a- and b-values and rain rates into temperature intervals, a clear linear relationship was evident

between a-and b-values for a-values in the range of 5-20. Separating into temperature intervals also showed that the spread among a-values increased with increased temperature, and higher temperatures showed in general increased values of b. However, an obvious relationship between rain rates and a-and b-values were also not evident for the individual temperature intervals.

This was also confirmed by table 4.1 where mean and median values of a and b are shown for different rain rates. The highest mean a-value can be found at a rain rate of 8 –10 mm/3h, with lower values for higher rain rates (see also table 6.1). The highest precipitation rates gave the lowest mean and median b-values. The highest mean and median b-values were found at rain rates of 6 –8 mm/3h with values around 1.2.

When averaging the overall a-values for the different temperature intervals, a relationship between rain rates and a-values was observed. The lowest temperatures had the lowest mean and median values of a with increasing values for increasing temperatures. The maximum mean a-value was found to be 193 at a temperature of 6 –9 °C. The same pattern was observed for the mean b-values, with a maximum average value of 1.13 at temperatures above 9 °C.

By separating and averaging over different wind speed intervals at Ulriken a distinct pattern was found. The mean and median a- and b-values were lowest at calm winds, with increasing values for increasing wind speeds.

Average a-and b-values when separated by wind direction at Ulriken provided no obvious pattern. However, the largest values were found at south/southwesterly winds and lowest values at north/northeasterly wind. (See also table 4.1 and 6.2).

The case studies showed a great variation among a- and b-values on a time scale of 1 h for the specific rain events. a shows a distinct wave-like structure with a period of typically 6 –8 h. In two out of three cases the a-value seems to be positively correlated with the amount of precipitation, in one case no relationship between values of a and rain rates are evident at all.

The value of b seems to be negatively correlated with the rain rate in one of the case studies, a slight positive correlation was seen in one case and no relationship was evident between the value of b and the rain rate in the third case.

There were no clear relationship between a-and b-values in two of the

cases, except for the occurrence of the lowest b-values both for very low and very high values of a in one of these cases. The third case showed a relationship between a and b similar to the overall three year relationship (top panel of figure 4.11) where a rapid increase in b is evident for a-values below 30. Between a-values of 30 to 300 the value of b is relatively constant between 1 and 1.5. However, the decreasing values of b in this case, for a-values above 300 is not evident in the overall three year relationship between a- and b-values.

In case 1 the arrival of a warmer air mass caused increasing a- and b-values. This also happened in case 2 when the bright band altitude increased early in the morning. In case 3 the passage of a cold front caused the a-value to increase and the b-value to decrease. However, there is no clear conclusion that the relationship between a and b is the opposite in cold vs. warm air.

The overall mean and median values of a and b in the Z-R relationships, $Z = aR^b$, found in this thesis can not fully confirm the reported values in table 2.2. The a-values are generally in the mid-range, but the b-values are on average low compared to those presented in table 2.2. One reason for this could be the high observed variability among the b-values on 1 h basis. When averaging over a longer time period (24 h, 48 h) all the low values will pull the average down. If the averages were made over a shorter time period it would probably fit better with the literature. In most of the publications on the Z-R relationship no information on the measurement or averaging intervals are given. The complex topography of the area around GFI and Florida, and vertical velocities of the air could also be potential reasons for why the relationships in table 2.2 could not be fully confirmed.

Based on the results of the presented master project some future MRR related activities can be proposed. It would be very interesting to have a closer look into the profiles of droplet size distributions at different altitudes instead of the reflectivity at one level as done so far. This could provide a better understanding of the microphysical processes, as evaporation, condensation and coalescence, and potentially also the effect of vertical velocity in complex terrain. This cluld help to clarify why the measurements in Bergen are not fully in agreement with the Z-R relationships published in the literature.

To investigate the influence of the complex topography even further, the installation of two more MRRs would be desirable. One unit upstream of the mean wind direction, e.g. at the western part of Sotra, and one downstream in

the mountains would provide an unique dataset on the effect of topography on precipitation microphysics.

Finally it could be an idea to couple the instantaneous Z-R ratios from the MRR with the reflectivity measured by the horizontally scanning rain radar system from MET Norway to enable a more quantitative determination of areal precipitation would also be useful. This could lead to more accurate precipitation measurements by horizontal scanning radars.

***a*-values, separated by:**	**Comments**
Temperature at Florida	Increasing a-value with increasing temperature. Maximum average value at a temperature of 6 –9 °C. Decreases a little bit when the temperature goes above 9 °C
Rain rate at Florida	The average a-value increases up to a rain rate of 8 –10 mm/3h. No specific pattern at higher rain rates. The lowest average a-value is found at a rain rate of 15 –20 mm/3h. Lowest value when looking at the median is found at 20 –40 mm/3h and highest at 6 –8 mm/3h.
Wind speed at Ulriken	Agreement between the average value and the median. Lowest value at calm winds. Increases with increasing wind speed. Maximum average value of 227.27 and maximum median of 239.19 at wind speeds over 20 $\mathrm{m\,s^{-1}}$.
Wind direction at Ulriken	No obvious pattern. Highest a-values at south/southwesterly winds. Lowest values at north/northeasterly winds.

Table 6.1: Summary of the mean and median a-values in table 4.1.

b-values, separated by:	Comments
Temperature at Florida	Mean and median agrees. The lowest temperature has the lowest *b*-value. Increasing values with increasing temperature.
Rain rate at Florida	The pattern of mean values is increasing and then decreasing. The highest precipitation rate gives the lowest values of *b*, but the lowest rain rate does not give the highest *b*-values. The highest mean and median *b*-values are found at a rain rates of $6-8\,\mathrm{mm/3h}$.
Wind speed at Ulriken	Lowest *b*-values at calm winds. Appears to rise with increasing wind speed both when looking at the mean and median. However, the median value stabilises at 1.11 at a wind speed of $10-15\,\mathrm{m\,s^{-1}}$ and keeps this value for higher wind speeds.
Wind direction at Ulriken	Does not provide an obvious pattern. South/southwesterly wind gives the highest *b*-value. Lowest *b*-value is found at north/northeasterly wind.

Table 6.2: Summary of the mean and median *b*-values in table 4.1.

Bibliography

Atlas, D. (1957), 'Drop size and radar structure of a precipitation streamer.', *Journal of Atmospheric Sciences* **14**, 261–271.

Austin, P. M. (1987), 'Relation between measured radar reflectivity and surface rainfall', *Monthly Weather Review* **115**(5), 1053–1070.

Battan, L. J. (1973), 'Radar observation of the atmosphere'.

Beard, K. (1976), 'Terminal velocity and shape of cloud and precipitation drops aloft', *J. Atmos. Sci* **33**(5), 851–864.

Clark, M. P. and Slater, A. G. (2006), 'Probabilistic quantitative precipitation estimation in complex terrain', *Journal of Hydrometeorology* **7**(1), 3–22.

Crochet, P., Jóhannesson, T., Sigurðsson, O., Björnsson, H. and Pálsson, F. (2008), 'Modeling precipitation over complex terrain in iceland', *Sveinsson, Ó. GB, SM Garðarsson and S. Gunnlaugsdóttir* pp. 11–13.

Duchon, C. E. and Essenberg, G. R. (2001), 'Comparative rainfall observations from pit and aboveground rain gauges with and without wind shields', *Water Resources Research* **37**(12), 3253–3263.

Fournier, J. D. (1999), 'Reflectivity-rainfall rate relationships in operational meteorology'.
URL: *http://www.srh.noaa.gov/tae/?n=research-zrpaper*

Fujiwara, M. (1967), 'Raindrop size distribution in warm rain as measured in hawaii', *Tellus* **19**(3), 392–402.

Geofysisk Institutt (n.d.), 'Nedbør'. Visited on 19.11.13.
URL: `http://veret.gfi.uib.no/?action=today&prod=11`

Geonor (n.d.), 'Geonor t-200b series, all-weather precipitation gauges'. Pdf downloaded from:.
URL: *http://www.geonor.no/index.php?option=com_content&view=article&id=21&Itemid=23&lang=no*

Gunn, R. and Kinzer, G. (1949), 'The terminal velocity of fall for water droplets in stagnant air.', *Journal of Atmospheric Sciences* **6**, 243–248.

Haby, J. (n.d.), 'What is bright band and how does it occur'. Visited on: 02.04.2013.
URL: *http://www.theweatherprediction.com/habyhints2/383/*

Huggel, A., Schmid, W. and Waldvogel, A. (1996), 'Raindrop size distributions and the radar bright band', *Journal of Applied Meteorology* **35**(10), 1688–1701.

Klaassen, W. (1988), 'Radar observations and simulation of the melting layer of precipitation', *Journal of the atmospheric sciences* **45**(24), 3741–3753.

Kneifel, S., Maahn, M., Peters, G. and Simmer, C. (2011), 'Observation of snowfall with a low-power fm-cw k-band radar (micro rain radar)', *Meteorology and Atmospheric Physics* **113**(1), 75–87.

Kumar, L. S., Lee, Y. H., Yeo, J. X. and Ong, J. T. (2011), 'Tropical rain classification and estimation of rain from zr (reflectivity-rain rate) relationships', *Progress in Electromagnetics Research B* **32**, 107–127.

List, R. (1988), 'A linear radar reflectivity-rainrate relationship for steady tropical rain', *Journal of the atmospheric sciences* **45**(23), 3564–3572.

Marshall, J. and Palmer, W. (1948), 'The distribution of raindrops with size', *Journal of meteorology* **5**(4), 165–166.

McNoldy, B. (2003), 'Radar meteorology tutorial'. Available at: *http://servv89pn0aj.sn.sourcedns.com/gbpprorg/mil/radar/Radar_Meteorology_Tutorial.pdf*.

Mendenhall III, W., Beaver, R. J. and Beaver, B. M. (2006), *Introduction to probability and statistics*, Cengage Learning.

METEK (2004), *Micro Rain Radar User Manual*. The manual was inculded with the instument. Version: x.14/x.30.

Nešpor, V. and Sevruk, B. (1999), 'Estimation of wind-induced error of rainfall gauge measurements using a numerical simulation', *Journal of Atmospheric and Oceanic Technology* **16**(4), 450–464.

Stout, G. E. and Mueller, E. A. (1968), 'Survey of relationships between rainfall rate and radar reflectivity in the measurement of precipitation', *Journal of Applied Meteorology* **7**, 465–474.

Uijlenhoet, R. and Pomeroy, J. (2001), 'Raindrop size distributions and radar reflectivity? rain rate relationships for radar hydrology', *Hydrology and Earth System Sciences Discussions* **5**(4), 615–628.

Waldvogel, A. (1974), 'The n 0 jump of raindrop spectra', *Journal of the Atmospheric Sciences* **31**(4), 1067–1078.

Wallace, J. M., Wallace, J. M. and Hobbs, P. V. (2006), *Atmospheric science: an introductory survey*, Vol. 92, Academic press.

Wilson, J. W. and Brandes, E. A. (1979), 'Radar measurement of rainfall-a summary', *Bulletin of the American Meteorological Society* **60**(9), 1048–1058.

Young, C. B., Nelson, B. R., Bradley, A. A., Smith, J. A., Peters-Lidard, C. D., Kruger, A. and Baeck, M. L. (1999), 'An evaluation of nexrad precipitation estimates in complex terrain', *Journal of Geophysical Research: Atmospheres (1984–2012)* **104**(D16), 19691–19703.